Hydraulic Pressure Ripple Energy Harvesting: Structures, Materials and Applications

Huifang Xiao[a], *Min Pan*[b], *Jun Yu Harry Chu*[b], *Chris R Bowen*[b,*], *Sebastian Bader*[c], *Javier Aranda*[c], *Meiling Zhu*[d]

[a] School of Mechanical Engineering, University of Science and Technology Beijing, Beijing 100083, PR China

[b] Department of Mechanical Engineering, University of Bath, Bath, BA2 7AY, United Kingdom

[c] Department of Electronics Design, Mid Sweden University, Holmgatan 10, 85170 Sundsvall, Sweden

[d] College of Engineering, Mathematics and Physical Sciences, University of Exeter, Exeter, EX4 4QF, United Kingdom

*Corresponding author. E-mail address: msscrb@bath.ac.uk (Chris R Bowen).

Keywords: Hydraulic pressure ripples, Energy Harvesting, Electroactive materials, Device architectures

Abstract

The need for wireless condition monitoring and control of hydraulic systems in an autonomous and battery-free manner is attracting increasing attention in an effort to provide improved sensing functionality, monitor system health and avoid catastrophic failures. The potential to harvest energy from hydraulic pressure ripples and noise is particularly attractive since they inherently have a high energy intensity, which is associated with the hydraulic mean pressure and flow rate. This paper presents a comprehensive overview of the state-of-the-art in hydraulic pressure energy harvesting, which includes the fundamentals of pressure ripples in hydraulic systems, the choice of electroactive materials and device structures, and the influence of the fluid-mechanical interface. In addition, novel approaches for improving the harvested energy and potential applications for the technology are discussed, and future research directions are proposed and outlined.

1. Introduction

Energy harvesting is a process of converting ambient forms of energy from our surroundings into usable electrical energy, which can act as a sustainable power source for low power electronic devices such as autonomous wireless sensors and portable electronic devices.[1-5] In hydraulic systems and environments, the continuous monitoring of industrial process parameters, such as pressure, temperature and vibration is of importance in an effort to monitor system health and avoid possible catastrophic failures. The potential for harvesting energy from hydraulic systems is particularly attractive since they inherently have a high energy intensity associated with the high mean pressure and flow.[6] Pressure fluctuations, and the induced acoustic noise that is accompanied with the mean pressure, are undesirable consequences of system operation and are generated in almost all pressurized fluid systems. The ability to generate usable electrical energy from such pressure fluctuations in hydraulic systems provides a route to enable autonomous and battery-free operation of low-power sensor nodes, thereby eliminating the need for battery management or reducing system complexity by removing the need for electrical power cables.

Hydraulic pressure energy harvesting (HPEH) has received increasing attention over the last decade. Studies to date have aimed to apply vibration harvesting technologies to a range of hydraulic environments. This review provides a comprehensive overview of the state-of-the-art in this emerging area, beginning with the fundamentals of pressure ripple harvesting and then overviewing typical harvester configurations, device architectures, tuning of the fluid to mechanical interface, selection of appropriate electro-active materials, and methods to improve output performance. We will also explore current progress and potential directions for performance enhancement to guide future research and promote future applications of hydraulic pressure energy harvesting.

2. Fundamentals of hydraulic pressure energy harvesting (HPEH)

Since the aim of HPEH is to harvest pressure fluctuations that are often present in pressurized fluid systems, we will first examine the origin of flow ripples, fluid-borne noise, and pressure ripples in hydraulic systems.

2.1 Characteristics of hydraulic systems

Hydraulic pressure ripples are caused primarily by unsteady flow from both pumps and motors, and the instability and cavitation events produced by valves.[7] As an example, hydraulic *flow ripples* can be produced in both the suction and discharge ports of a pump, as shown in **Figure 1(a),** which combines with the characteristics of the connected hydraulic circuit to produce pressure ripples.[8] The *pressure ripple* is defined as the acoustic, or dynamic, peak-to-peak amplitude that fluctuates about the mean of the pressure in a hydraulic system. It is these pressure ripples that are to be harvested in HPEH. Such pressure ripples are observed as *fluid-borne noise* (FBN) which can propagate long distances along fluid pipelines, thereby transmitting noise from the pump or motor to various parts of the hydraulic system. Fluid-borne noise can lead to unwanted *structure-borne noise* (SBN) and *air-borne noise* (ABN).[9]

A common source of pressure ripples is *positive displacement* pumps, which produce a periodic waveform flow that consists of a mean flow value with a superimposed flow ripple.[10] Examples include external gear pumps, axial piston pumps and screw pumps, which have a positive displacement to drive flow out from an inlet to an outlet. The discharge flowrate from a positive displacement pump is unsteady due to the discrete flows from each piston, gear tooth or vane, which consists of a mean flow rate with a superimposed periodic fluctuation. The flow ripple interacts with the characteristics of the hydraulic circuits to produce a pressure ripple.

The magnitude of the flow ripple is dependent upon the pump type and operating conditions, but it usually has a peak-to-peak amplitude of between 1 and 10% of the mean flow rate.[8,11] To measure the pump flow ripple and fluid borne noise characteristics the “secondary source” (SS) method (ISO 10767-1: 1996) [11-14] and the “2 pressures / 2 systems” (2P2S) method (ISO 10767-1: 2015) [15] are used. The 2P2S method has recently replaced the secondary source as the ISO standard for precision testing, although the UK has retained the SS method for its BS ISO standard.

Each type of pump produces pressure ripples with specific characteristics. In general, external gear pumps and axial piston pumps produce high flow ripples and high pressure ripples, while screw pumps produce low flow ripples and low pressure ripples. Axial piston pumps are widely used in high-performance hydraulic systems in aerospace, automotive, and construction and agricultural machinery for their variable capacities and high operating pressures. The flow ripple from an axial piston pump is the sum of individual cylinder flows, and its magnitude is dependent on the design of the pump and the port plate geometry.

A simple hydraulic circuit that consists of a pump, a rigid pipe, and a restrictor valve is shown in **Figure 1(b)**. The pump generates a flow ripple that consists of a broad spectrum of harmonic components with a fundamental frequency that is determined by the speed and geometry of the pump. The flow ripple can be separated into a series of sinusoidal components using Fourier analysis in the frequency domain. These consist of a fundamental component at the pumping frequency and higher harmonics at integer multiples of the fundamental frequency. The fundamental frequency is equal to the pumping frequency, which is the speed of the pump (in revolutions/second) multiplied by the number of pistons or gear teeth.[8] For example, a gear pump with nine teeth, driven by a motor speed of 3600 rpm, will generate pressure ripples at a fundamental frequency, f = (3600×9)/60 = 540 Hz. Higher frequency harmonics (such as 1080 Hz, 1620 Hz etc.) are also to be produced, but will be of lower amplitude and energy. Examples of pressures and frequencies examined to date for hydraulic energy harvesting will be described later in the review (Section 5).

The hydraulic flow ripple interacts with the system, thereby producing a complex pressure ripple which is superimposed upon the mean system pressure. This pressure wave is then propagated along the pipeline at the speed of sound. When the pressure wave encounters a discontinuity, such as a valve or load, it is partially reflected towards the pump. For example, in a simple hydraulic circuit, as shown in **Figure 1(b)**, when the pressure wave reaches the valve end of the pipe, the wave is reflected and travels back to the pump. When the reflected pressure wave reaches to the pump, it is reflected again and may combine with the original wave to reinforce the original valve and form a resonant condition. With further reflections

and the subsequent pressure waves from the pump, the system has two sets of travelling pressure waves. One set travelling away from the pump, namely, the pressure ripple *progressive* wave, and the other set travelling in the reverse direction, namely the pressure ripple *regressive* wave. The progressive and regressive waves interfere with each other and produce a standing wave of the pressure ripple, and a resonant condition occurs due to the nature of the conciliation of the pressure ripple. Therefore, the length of the pipe has a significant effect on the pressure ripples in hydraulic systems. **Figure 1(c)** shows measured flow ripples of a gear pump working at a mean pressure of 200 bars for two different hydraulic circuits of the volume-termination circuit (VT) and restriction-termination circuit (RT). The VT circuit that operates with a high pressure results in a large flow ripple, while the RT circuit that operates with a lower pressure results in a relatively small flow ripple.[10] The troughs in the flow result from the pump type, operating conditions, and fluid compression. The magnitude of the flow ripple is approximately proportional to system operating pressure,[10] indicating that higher pressure hydraulics provide opportunities for higher harvested power.

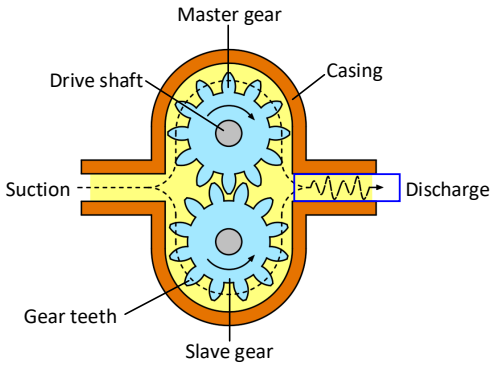

(a)

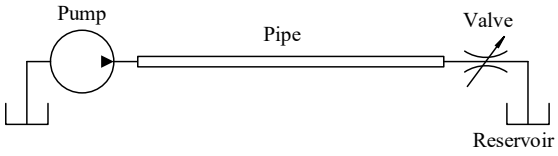

(b)

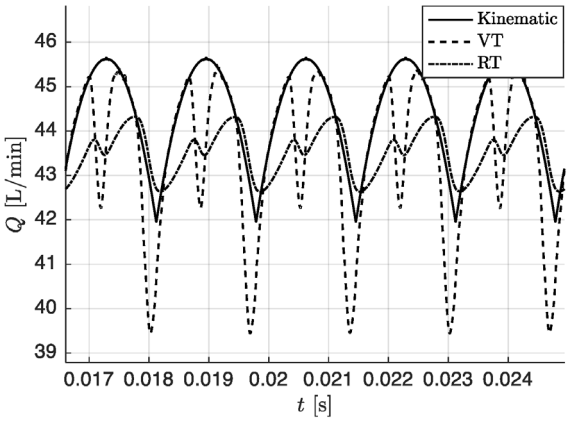

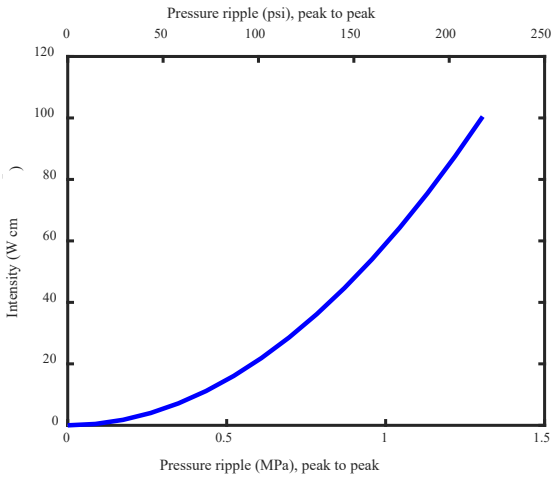

(c) (d)

Figure 1. (a) The generated flow ripple in a gear pump. (b) Schematic of a hydraulic pump-pipe-reservoir circuit. (c) Example of measured flow ripples of a gear pump. Reproduced under the terms of the CC-BY license. [10] Copyright 2019, MDPI. (d) Power intensity of a hydraulic system with pressure ripple, determined by **Equation (1)**.

Digital hydraulic components or systems such as digital pumps, valves and actuators, and switched inertance hydraulic converters all promise high-energy efficiency, but also generate high-pressure ripples.[16] This is primarily caused by the high frequency switching between different hydraulic flow sources when using high-speed digital valves. The magnitude of the flow ripple is determined by the pressure difference between the different supply sources. Severe cavitation may also occur when the pressure ripple is extremely high. In the fluid power community, attenuation of pressure ripples is a highly important research area for creating quiet and highly efficient hydraulic machines and systems. A wide range of FBN silencers, attenuators and pulsation dampers are developed for this purpose. These *passive* FBN attenuation devices can be highly effective in reducing the FBN, with a typical reduction of 20 to 40 dB.[8] *Active* FBN control techniques with advanced control algorithms have also been developed for FBN attenuation in conventional and digital hydraulic systems,[17-22] but they are still in their infancy. The high energy of structure-borne noise as a result of FBN can lead to failures in aircraft hydraulic systems due to the excitation of high-density fluid fluctuations and the nature of the vibrational environment of the airframe. For further information, the reader is referred to a comprehensive overview of existing vibration control techniques of hydraulic pipeline systems by Gao *et al*;[23] practical recommendations for applying vibration control technologies have been provided for improving reliability and reducing pressure ripples, to minimize the risk of failure in the overall system. The potential to reduce noise while simultaneously generating power for autonomous sensor nodes by energy harvesting is therefore an attractive alternative to passive or active attenuation methods.

2.2 Power intensity of pressure ripple in hydraulic systems

The high power intensity of pressure ripples in hydraulic systems provides a significant opportunity for energy harvesting for self-powered wireless sensors for applications, such as structural health monitoring and prognosis. We have seen that hydraulic systems operate with high mean pressure and flow, and the presence of dynamic pressure ripple can be extracted as a source of acoustic energy and then converted to electrical energy for self-powered devices. To design an energy harvesting device using the power generated by the hydraulic pressure ripple, the power intensity is usually calculated by quantifying the energy input for the energy harvester. The *power intensity I* (W cm^{-2}) of pressure ripples is based on the magnitude of the pressure wave and is defined as;

$$I = \frac{P_{ripple}^2}{2\rho c} \tag{1}$$

where c is the speed of sound, ρ is the density of the hydraulic fluid and P_{ripple} is the magnitude of the dynamic pressure ripple. Assuming a dynamic pressure ripple peak-to-peak amplitude of P_{ripple} = 10 bar (~1 MPa) with a hydraulic fluid density of ρ = 800 kg m^{-3} and speed of sound of c = 1400 m s^{-1}, the power intensity of the pressure ripple is 45 W cm^{-2}, which represents a high-energy-intensity source that can be converted into electrical power by an energy harvesting system. This is a stark contrast to the power intensity of acoustic waves with <1 μW cm^{-2}.[24] **Figure 1(d)** shows the variation of power intensity with pressure ripple, as determined by **Equation (1),** which demonstrates that the power intensity is proportional to P_{ripple}^2. The power intensity of pressure ripples for a hydraulic system driven by an axial piston pump at a fundamental frequency of 270 Hz has also been reported. [25]

As an example, Cunefare *et al.*[26] fabricated a prototype energy harvester to generate electrical power from hydraulic pressure ripples, which powered sustainable wireless sensor nodes and electronic systems for structural health monitoring. The first prototype employed an axially poled commercial piezoelectric multi-layer stack, as shown in **Figure 2**, where a piezoelectric stack (6.8 mm × 6.8 mm × 30 mm) was attached to the hydraulic pipe with a 0.0762 mm thick aluminum diaphragm interface, which provided a fluid-mechanical coupling between the piezoelectric stack and pressure ripple. The alternating stress applied to the piezoelectric stack due to the hydraulic pressure ripple can be controlled by adjusting the

effective area of the stack; the impact of materials and stack geometry will be described in more detail later (Section 3.3 and Section 4). A nine-piston axial piston pump was used as a hydraulic power source with an operating speed at 1500 rpm and a fundamental frequency of f = (1500 × 9)/ 60 = 225 Hz. The prototype provided a maximum power output of up to 1.2 mW from a dynamic pressure ripple of P_{ripple} = 4 bar (~ 0.4 MPa). It was demonstrated that the power generated was viable for typical wireless self-powered sensing applications, which can effectively reduce the need for instrumentation wires and power supplies such as batteries. This energy harvester prototype has the potential to operate with higher pressure ripples for the generation of higher electrical power.[26,27] The resonance frequency of piezoelectric stacks is typically in the kHz range and therefore much higher than the dominant pressure frequencies with hydraulic systems. Therefore, the hydraulic pressure energy harvesters are usually *non-resonant* energy harvesting systems; examples of resonant based systems will be described in Section 4.

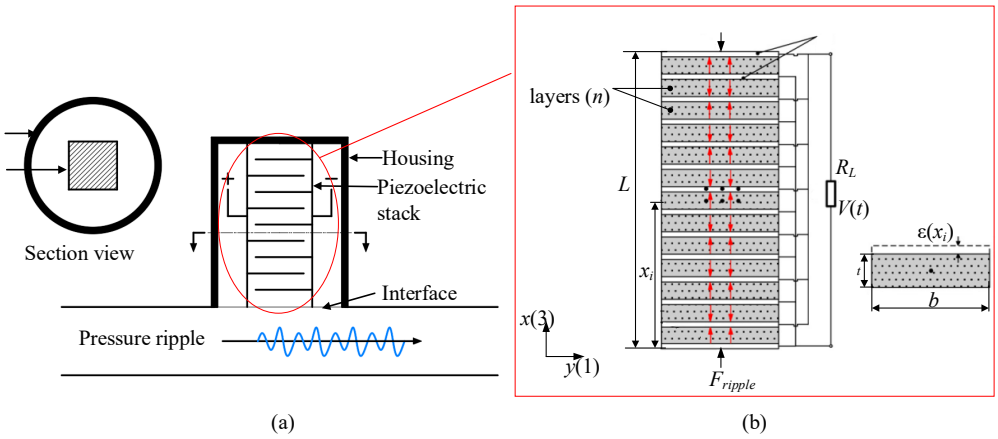

Figure 2. (a) Schematic of a hydraulic pressure energy harvester with piezoelectric stack, (b) Schematic of stack showing the multilayer structure and the electro-mechanical coupling model of the piezoelectric stack with n layers, V is voltage, R_L is load resistance, F_{ripple} is time-varying force, L is stack length, and t is piezoelectric layer thickness.

The key contributing factors for optimizing the power density output (power per unit volume) from dynamic pressure ripples by hydraulic energy harvesters are:

(i) the fluid-mechanical coupling between the piezoelectric stack and pressure ripples,

(ii) the ratio of the effective contact area of the resulting force from the dynamic pressure to the cross-sectional area of the piezoelectric stack,

(iii) the flexibility of the fluid-mechanical coupling interface and the maximum surface deflection without damaging the piezoelectric stack or diaphragm; failure of the piezoelectric material can correspond to fracture, fatigue, or loss of piezoelectric activity due to depolarization of the material at high levels of stress.

To improve the performance and power density, a range of energy harvesting prototypes for operation at high static pressure levels and high pressure ripples have been developed and investigated. The highest power density has been achieved using single-crystal ferroelectric materials, primarily due to the high piezoelectric charge coefficients (d_{ij}) of the materials employed.[28,29] Schwartz *el al*.[6] demonstrated a proof-of-concept hydraulic energy harvester in a hydraulic circuit. The harvester successfully generated 2.6 mW, which powered a two-parameter sensor using radio frequency communication at a sampling rate of up to 333 Hz. Given the increasing availability of a variety of energy-harvesting-targeted microcontroller units (MCU) and low-power communication, hydraulic pressure energy harvesters appear to be a viable energy source for implementing "Internet of Things" wireless sensing systems that utilize hydraulic fluid power systems. Toothman *et al.*[30] further enhanced the implementation of the hydraulic energy harvester by connecting it with a new communication system that allowed it to store energy and communicate sensor readings via Bluetooth Low Energy (BLE).

For low dynamic pressure ripple conditions with a reduced power intensity, Skow *et al.*[29] studied the feasibility of energy harvesting in low dynamic pressure environments, such as cross-country pipelines and water distribution networks operating at much lower static pressures of approximately 1 to 4 MPa. An electromechanical model and a hydraulic pressure energy harvester prototype based on a ferroelectric single-crystal were developed to demonstrate the potential of the technology.

Alternatively, the hydraulic accumulator is a device that stores energy in the form of fluid pressure, which can be released intermittently as required. Liu *et al.* [31] designed a novel hydraulic accumulator with a large energy storage capacity and high controllability and investigated its impact on system performance. The energy-storage capacity of the new

accumulator can be improved by approximately 1.5 times, compared to the conventional accumulators. Using a Fuzzy PID (proportional integral derivative) control algorithm, the pre-charge pressure, output flow and pressure of the accumulator could be effectively controlled. The high energy-storage capacity and fast response of this new accumulator has potential for energy harvesting applications; for example, Nie *et al.*[32] introduced piezoelectric materials into an accumulator to convert pressure variations into electrical energy.

Now that the fundamental characteristics of hydraulic systems and the origin of pressure ripples have been described, specific examples of harvesting from hydraulic pressure systems are examined in more detail.

2.3 Energy harvesting from hydraulic pressure systems

We have seen that hydraulic systems are inherently high mean pressure and flow, which can reach pressures of up to 35 MPa,[33] and the dynamic pressure ripple accompanied with the mean pressure is of high power intensity and can be approximated as 10% of the mean pressure.[33] For example, for a modern large hydraulic motor, where the speed of sound is 1400 m s^{-1}, the fluid density is 800 kg m^{-3} and the mean working pressure is 35 MPa, the pressure ripple is 3.5 MPa and the energy intensity level of the system, from **Equation (1)**, is 547 W cm^{-2}.

Energy conversion of the pressure ripples into electrical energy using hydraulic pressure energy harvesters (HPEH) is commonly achieved via the excitation of an electroactive material, such as a piezoelectric or magnetostrictive. The dynamic pressure ripples are transferred into the electroactive material through a fluid to mechanical interface. In early studies, a bluff body-polyvinylidene fluoride (PVDF) piezoelectric polymer membrane configuration was proposed to transfer the flow-induced vibrations into electrical energy via the piezoelectric effect.[34] An alternative conversion mechanism based on piezoelectric cantilevers was also utilized for energy harvesting from pressurized flow excitations.[35] We have seen from **Equation (1)** and **Figure 1(d)** that since the power intensity is proportional

to P_{ripple}^2, it is beneficial if the available pressure ripples are large. Since the harvester should be capable of sustaining large pressure loads without failure or a decrease in performance, Cunefare *et al.* [26] proposed a prototype of a hydraulic pressure energy harvester that used a ceramic piezoelectric multilayer stack to convert pressure ripples into electrical energy, which has been used widely in the literature as a benchmark for performance comparison and improvement, as shown in **Figure 2(a)**. A piezoelectric stack, which is formed from multiple layers of piezoelectric ceramic disks or layers, as shown in **Figure 2(b)**, has a high equivalent piezoelectric charge coefficient compared to a single layer piezoelectric plate.[36-38] Based on an electro-mechanical coupling model of the piezoelectric stack, **Figure 2(b),** the open-circuit output power obtained by a piezoelectric stack under a dynamic compression can be expressed as [37]

$$P(\mathrm{t}) = \frac{\omega d_{eq}^2 F_{ripple}^2}{2C_{eq}} \sin(2\omega \mathrm{t} - 2\Delta\phi) \tag{2}$$

where ω is the pressure ripple frequency in radians, d_{eq} is the equivalent piezoelectric charge coefficient of the piezoelectric device, F_{ripple} is the amplitude of the force acting on the piezoelectric stack due to the pressure ripple and C_{eq} is the effective capacitance of the piezoelectric element. For a piezoelectric stack with n active layers connected in parallel, assuming each layer has the same piezoelectric charge coefficient d_{33} (a measure of the charge per unit force) and capacitance C_p, the equivalent piezoelectric coefficient and effective capacitance of the stack can be expressed as

$$d_{eq} = nd_{33}, \quad C_{eq} = nC_p \tag{3}$$

The high stiffness and relatively high compressive strength of the ceramic piezoelectric stack in the axial direction allows it to withstand relatively high pressures of up to 40 MPa [39] and are now the most suitable configuration for high-pressure energy harvesting in hydraulic systems. We will see later that the maximum allowable pressure on the stack is not only determined by the compressive or fatigue strength of the ceramic, but also the depolarization stress of the material; also termed the *coercive stress*.

The piezoelectric stack is exposed to hydraulic pressure ripples in the fluid system through a fluid to mechanical interface which acts to isolate the stack from the fluid, while also allowing

pressure ripples to be strongly coupled into the stack. This process induces physical deflections of the piezoelectric ceramic and produces an electric potential across the electrodes due to the direct piezoelectric effect. The electrode terminals are connected to an external resistive load to complete an electric circuit and provide a current and power, as shown in **Figure 2(b)**. Therefore, the generated voltage and electrical power of the hydraulic pressure energy harvester is dependent on four factors: (i) structure of the ripple harvester; (ii) the fluid to mechanical interface; (iii) the piezoelectric material and its configuration; and (iv) the electrical load and power management circuits used to rectify and store the AC electrical output, as shown in **Figure 3**. The first three factors that influence performance and power are elaborated in detail in the following sections, beginning with the typical hydraulic pressure energy harvesting structures and configurations. As for the fourth factor of power management circuits, they are not specific to hydraulic pressure energy harvesting and thus we could refer to other relevant literature, such as for vibration energy harvesting. [40-43]

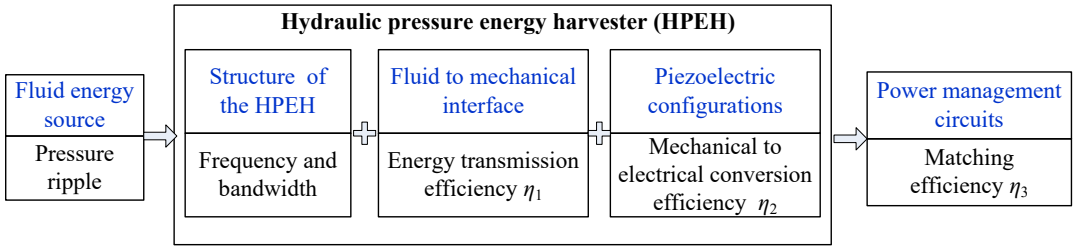

Figure 3. Factors related to the energy harvesting performance of hydraulic pressure energy harvesters.

3. Modeling and prototypes

3.1 Typical HPEH configurations and devices

The typical configuration of hydraulic pressure energy harvesters reported in the literature consists of three main components: (i) an interface between the hydraulic fluid and the transducer (ii) a smart-material that acts as the mechanical-to-electrical energy transducer, and (iii) an electrical load or power management circuit.

Figure 4 shows common configurations for hydraulic pressure energy harvesters. These include: (a) a transducer patch which consists of a fluid to mechanical interface and a bonded transducer, this can take the form of a piezoelectric patch or material on a metallic membrane

which interacts with the hydraulic fluid; (b) a hydraulic harvesting transducer with a back support; where the transducer is located inside a housing frame; (c) a supported transducer with a metallic spacer between the transducer and the fluid to mechanical interface to avoid a catastrophic stress in the plate under high pressure and (d) a hydraulic pressure energy harvester with a transducer subjected to a force that has been amplified by a mechanical frame [44].

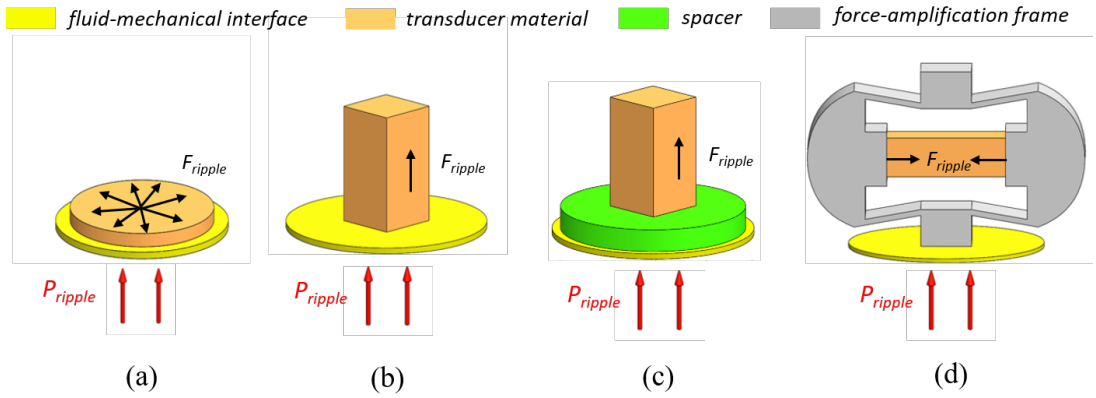

Figure 4. Common configurations for hydraulic pressure ripple energy harvesters: (a) Transducer patch with no support on the transducer, (b) Supported transducer, (c) Supported transducer with a spacer between the transducer and the fluid to mechanical interface, and (d) An example of a supported mechanical amplifier with an integrated transducer. Different colors represent different components, yellow: fluid-mechanical interface; orange: transducer material; green: spacer; grey: force amplification frame.

The primary role of the fluid-to-mechanical interface is that of protecting the transducer, sealing the hydraulic fluid, and converting the pressure ripples into a mechanical force that is applied to the energy harvesting transducer. The transducer, integrated into the fluid-to-mechanical interface, or separated from it, converts the mechanical energy into electrical energy. Both the transducer and interface should be designed to endure the static compression pressure exerted by the fluid. The type of configuration used for a given application is dependent on the static pressure. Applications with low static pressure, or where the size of the fluid-to-mechanical interface does not result in high forces, can employ HPEH configurations with unsupported transducers, such as in **Figure 4(a)**, or with mechanically amplified transducers, as in **Figure 4(d)**. Back-supported transducer configurations, such as

those in **Figure 4(b) and (c)** can exhibit improved endurance for operation in high-pressure systems, with the supported transducer with spacer configuration being the most common configuration in high-pressure systems.[45,46] Furthermore, if the application allows, the transducer and interface configuration can be designed to be compliant with the hydraulic fluid and match the resonant frequency to the dominant frequency of the pressure ripple.

Previous studies on HPEHs have primarily employed piezoelectric devices as the main transducer element. A variety of ceramic multi-layer piezoelectric stacks has been employed as the harvesting transducer. [26, 44-46] These transducers have often been selected due to their high compressive strength and good electromechanical transduction performance; for example, Aranda *et al.* [47,48] employed multi-layer piezoelectric stacks for their studies. These types of transducers, commonly used in positioning applications as low voltage and high precision actuators, are commercially available, although it should be highlighted that these devices are optimized in terms of choice of piezoelectric material and device geometry for high *actuation* strain, rather than for energy harvesting under high stress. The factors that impact the selection of a piezoelectric stack are, amongst others, the constraints of maximum static pressure, area, length, temperature, and cost. Commonly, a larger volume piezoelectric stack can yield higher power for a given pressure ripple and full design considerations must be taken into account, and a more detailed evaluation is undertaken in Section 3.3. In addition to the energy harvesting configuration, the fluid to mechanical interface is of importance and is now described.

3.2 Fluid to mechanical interface

The *fluid to mechanical interface* is an important component of a hydraulic pressure energy harvester since the interface acts to convert the pressure ripple into an alternating mechanical force to deform the piezoelectric element, while protecting the piezoelectric material from the fluid. The coupling between the pressure ripples and mechanical forces and the resulting deformation mechanisms at the interface are important factors that determine the output energy, bandwidth, and conversion efficiency of the harvesting device.

Thin metallic circular edge-clamped flat plates have been used as the interface between the hydraulic fluid and piezoelectric stack, similar to that in conventional industrial pressure sensors. [49] To increase the efficiency of force transmission at the interface, the thickness of the plate is often thin, typically in the order of micrometers. [48,50] For example, the thickness of the flat metallic shim is 100μm in, [48] and the investigated plate thickness was in the range of 25μm to 100μm in. [50] The piezoelectric multi-layer stack is generally located at the center of the circular plate, as shown in **Figure 4(b)**, which acts as the mechanical to electrical transfer component. The hydraulic pressure created by the pressure ripple acting on the plate bends the circular plate and compresses the piezoelectric stack that is constrained by the housing, as shown in **Figure 5(a) and 5(b)**. Therefore, there are two external forces applied on the piezoelectric stack and the interface plate coupling structure that originate from (i) the reaction force from the upper housing on the piezoelectric stack and (ii) the dynamic pressure load from the ripple on the plate surface. The piezoelectric stack then generates a voltage and associated electrical energy due to the combined force and induced strain.

The area of the flat plate of the mechanical interface is generally larger than that of the piezoelectric stack to achieve an appropriate force transmission from the pressure ripple load applied to the plate and the force delivered to the piezoelectric stack. The alternating force F_{ripple} that acts on the exposed interface can be calculated as

$$F_{ripple} = P_{ripple} A_p \tag{4}$$

where P_{ripple} is the pressure amplitude of the ripple and A_p is the area of the plate exposed to the fluid. The ideal case is that the force applied to the interface plate are completely transmitted to the piezoelectric stack for power conversion by the direct piezoelectric effect. However, only a fraction of the force on the plate is transferred to the stack due to the energy loss in bending the plate and the coupling mechanism, thereby leading to a loss in efficiency. [39]

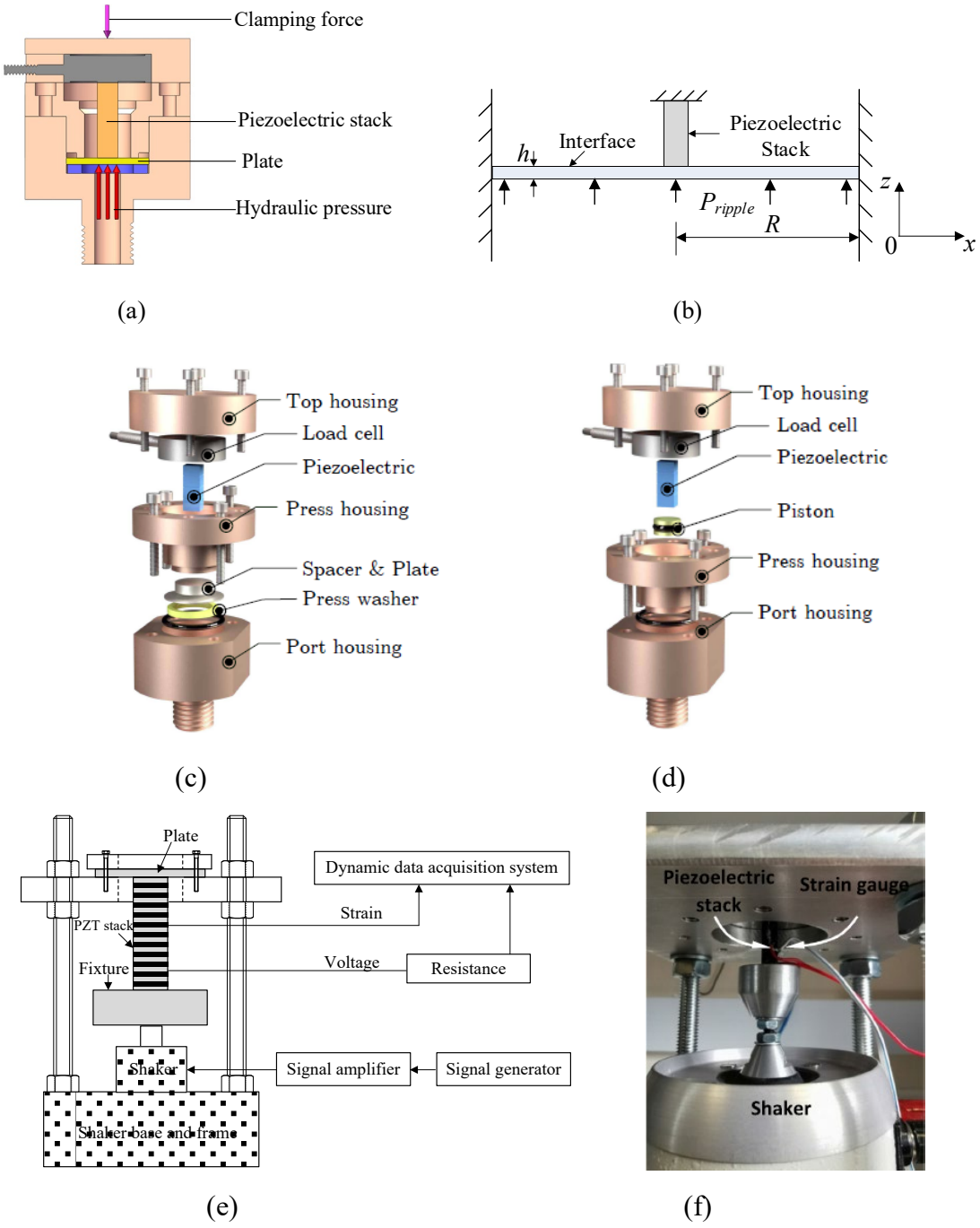

Figure 5. (a) Structure of the hydraulic energy harvesting device with piezoelectric stack. (b) Model of an edge-clamped flat plate interface with a central piezoelectric stack under the action of pressure ripple, (c) and (d) Assembly of the energy harvesting device with a flat plate and a piston as fluid to mechanical interface, respectively. Reproduced with permission.[47] Copyright 2018, IEEE. (e) Diagram of an experimental setup, (f) Detailed image of interface-piezoelectric stack structure. Reproduced with permission. [55] Copyright 2020, Elsevier Ltd.

Compared to the relatively large number of studies on the structural design of hydraulic pressure energy harvesters to improve the energy harvesting efficiency, the fluid to mechanical interface has yet to be studied in detail. With regard to the bending behavior of a circular edge-clamped flat plate, Way *et al.*[51] presented a general solution for the fundamental equations of a circular plate that is subjected to bending with a large deflection. Sheplak and Dugundji [52] investigated the large deflections of a clamped circular plate under an initial in-plane tension load and a uniform pressure applied over its surface. A continuous transition from plate behavior to membrane behavior was observed. Xue and Hu [53] studied the nonlinear behavior of a vibration energy harvester that consisted of a circular piezoelectric plate with a relatively large deflection near its natural resonance and applied electrical load resistance. Karagiozova *et al.* [54] proposed an approximated method to predict the large deflections of a clamped circular plate made of an elastic-perfectly plastic material when subjected to a uniform quasi-static pressure.

With regard to the stress transfer mechanisms of the fluid to mechanical interface in a hydraulic pressure energy harvester, Aranda *et al*. [39,47] analyzed the efficiency of force transmission of two different types of fluid to mechanical interfaces based on a flat metal plate and a conventional hydraulic piston using finite element simulations and experimental measurements. This is shown by the flat plate configuration in **Figure 5(c)**, which is a back-supported configuration with a spacer located between the piezoelectric stack and the fluid to mechanical interface as in **Figure 4(b)**, and a hydraulic piston in **Figure 5(d)**. The force transmission efficiency was defined as the ratio of the normal force on the piezoelectric stack to the force acting on the exposed interface area of the harvester. It was concluded that the force transmission efficiency is highly dependent on the operating pressure. Thin plates were shown to be good force coupling components for low-pressure systems, however they were deemed to be unsuitable for hydraulic systems with high-pressure levels due to the relatively smaller force transmission efficiency and the potential for mechanical yield, fatigue and mechanical failure of thin plates under the action of a high mean pressure.[39]

Recently, Xiao *et al.* [55] developed a generalized model of a hydraulic piezoelectric harvester

based on a circular edge-clamped flat plate interface with a central piezoelectric stack. The force-deflection relationship of a circular edge-clamped flat plate with a central lumped mass attachment was obtained and a cubic hardening nonlinear behavior was observed. The energy conversion efficiency of the system, which was defined as the ratio between the electrical energy output to the mechanical energy input was provided. **Figure 5(e) and (f)** show the experimental setup of the circular edge-clamped flat plate interface with a central piezoelectric stack. The piezoelectric stack was subjected to harmonic excitation, generated by an electromagnetic shaker to represent the harmonic pressure ripple in hydraulic systems. Thin flat plates of different thicknesses were used for measurements. It was shown experimentally that a decrease in plate thickness by a factor 2.5 reduced the output power by almost 50%; this was a result of the increased energy lost in bending the plate which acts as the interface. However, it was shown that a thin interface can be used to introduce a stronger degree of nonlinearity to increase the bandwidth to accommodate multiple frequency components and to improve the overall energy harvesting performance. This could be of particular advantage as the fundamental frequency of the ripple pressure is subjected to changes during service.

3.3 Figure of merit for selection of ripple harvesting materials and devices

Now that the range of harvester configurations and the fluid to mechanical interface has been described, it is interesting to consider the impact of the energy harvesting materials, and its geometry on performance. A range of materials and devices have been used for ripple harvesting, including ferroelectric piezoelectric materials in polymeric,[35] ceramic [26,27,39,44,55] and single-crystal form.[28,29] If the material is in bulk form, the material is commonly polarised in the thickness direction, as in **Figure 6(a)**, which leads to a screening charge on the electrode surfaces to balance the polarization. During a pressure ripple cycle, the application of a compressive stress to the piezoelectric material leads to a decrease in the level of polarization. As a result, some of the surface charge is now free to flow in an electrical circuit, as seen in the central image of **Figure 6(a)**. On removal of the compressive stress, the polarisation level of the material increases as it returns to its original (stress-free) level and the current will begin to flow in the opposite direction to rebalance the surface charge; see the

right image of **Figure 6(a)**.

We have seen that in many cases the harvesting element is a piezoelectric ceramic multi-layer stack, as shown in **Figure 2(b)**, which is typically manufactured from layers of lead zirconate titanate (PZT) ceramic[26,27] rather than a bulk monolithic material. In this case the piezoelectric device can be considered as multiple piezoelectric elements which are electrically connected in parallel, and there are multiple electrode surfaces to collect the piezoelectric charge as a result of a change in polarisation with applied stress. We will see later that the existence of multiple electrodes leads to more charge, but not necessarily more energy due to the lower voltage.

Xu *et al.*[36] have undertaken a detailed analysis of the use of piezoelectric stacks for energy harvesting, and we now examine their approach to identify potential materials and multi-layer structures of interest for ripple harvesting. In this mode of operation, the device operates in the longitudinal d_{33}-mode, which indicates that the applied load is parallel to the poling direction of the materials, and along the device length. The d_{33} piezoelectric charge coefficient provides a measure of the charge per unit force and is related to the change in polarization with stress.

We will initially consider a stack with a cross-sectional area A_s, length L, which consists of n multi-layers, each with a thickness t. It is assumed that the material is polarised along the device length and is operating off-resonance since the fundamental pressure ripple frequency is assumed to be much lower than the natural frequency of the harvester. It should be noted that the case $n = 1$ represents a harvesting element that consists of a single element, namely a bulk material. If an alternating load F_{ripple} is applied along the length of the device from the pressure ripple, the generated charge (Q) is given by

$$Q = nd_{33}F_{ripple} \tag{5}$$

where d_{33} is the piezoelectric charge constant (C N^{-1}) and is a property of the piezoelectric material. It can be seen that to generate a high piezoelectric charge per unit force (Q / F_{ripple}), there is a need to select materials with high d_{33}, and use a large number of multi-layers (n).

The capacitance (C) of a single layer in the multi-layer device can also be determined from

$$C = \frac{A_s \varepsilon_{33}^T \varepsilon_0}{t} \tag{6}$$

where ε_{33}^T is the relative permittivity at a constant stress of the piezoelectric material, and ε_0 is the permittivity of free space. For a multi-layer structure, there are n piezoelectric layers that are electrically connected in parallel. As a result, the total capacitance of the device is given by

$$C_{eq} = \frac{n A_s \varepsilon_{33}^T \varepsilon_0}{t} \tag{7}$$

Since $t = L/n$, we can also describe the capacitance by

$$C_{eq} = \frac{n^2 A_s \varepsilon_{33}^T \varepsilon_0}{L} \tag{8}$$

Therefore, a large device capacitance is achieved using material of high relative permittivity, a device structure with a large number of layers, or a large area. An increase in device length, while maintaining the same number of layers, leads to a reduction in device capacitance.

Since many ferroelectric polymers, ceramics, and single crystals are dielectrics, we can consider the device as a simple capacitor. The open-circuit voltage (V_{oc}) generated from an applied load can therefore be calculated from the relationship $Q = C_{eq} V_{oc}$. From **Equation (5)** and **(8)**, the open-circuit voltage generated from an applied force is, therefore,

$$V_{oc} = \frac{d_{33}}{\varepsilon_{33}^T \varepsilon_0} \frac{F_{ripple}}{A_s} \frac{L}{n} \tag{9}$$

The open-circuit voltage for a given applied ripple load and device geometry (A_s, L and n) can therefore be maximized by selecting materials with a high $g_{33} = d_{33} / \varepsilon_{33}^T \varepsilon_0$; this parameter is termed the *piezoelectric voltage constant* (g_{33}) since it is a measure of the electric field generated per unit stress. **Equation (9)** indicates that the open-circuit voltage for a particular material can be maximized using a device with a small area, a small number of layers, or a large length. Such a combination of geometrical factors leads to a low device capacitance, see **Equation (8)**, and a high open-circuit voltage for a specific level of charge since $Q = C_{eq} V_{oc}$.

In the context of energy harvesting, the energy (E) generated by the alternating load within a pressure ripple cycle is more important than the charge or voltage. This is estimated from the energy (E) stored in the capacitor, which is given by

$$E = \frac{1}{2} C_{eq} V_{oc}^2 = \frac{Q^2}{2C_{eq}} \tag{10}$$

This leads to

$$E = \frac{1}{2} \frac{F_{ripple}^2}{A_s} \frac{d_{33}^2}{\varepsilon_{33}^T \varepsilon_0} L \tag{11}$$

It should be highlighted that E represents the energy generated within a single ripple cycle, and the power ($P = Ef$) can be increased by increasing E or the ripple frequency (f). As a result of **Equation (11)**, for a fixed ripple force (F_{ripple}) and device geometry (A_s, L), to maximize the harvesting energy in a single force cycle, we can select piezoelectric materials with a high off-resonance harvesting figure of merit, FoM_{33}, where

$$FoM_{33} = \frac{d_{33}^2}{\varepsilon_{33}^T \varepsilon_0} \tag{12}$$

Priya[56] also took into account of electrical losses in the piezoelectric material during low-frequency energy harvesting by taking into account the dielectric loss (tanδ) of the material, this leads to;

$$FoM_{33} = \frac{d_{33}^2}{\varepsilon_{33}^T \varepsilon_0 \left(\tan \delta\right)} \tag{13}$$

For a given material, **Equation (11)** shows that a piezoelectric device with a small area and large length is also desirable, again since they both act to reduce the device capacitance. Interestingly, the number of layers in the multi-layer is not a factor with regards to the generated energy, and only influences the charge (**Equation (5)**) and open-circuit voltage (**Equation (9)**). This stems from the fact that $C_{eq} \propto n^2$, $Q^2 \propto n^2$, and $V_{oc}^2 \propto 1/n^2$, and the number of layers, therefore cancels out in **Equation (10)**.

Multi-layer piezoelectric devices are often used for ripple harvesting and while the presence of a large number of layers (n) does not increase the energy, there are some advantages of using a multi-layer piezoelectric structure compared to a single element/layer of ceramic

material. These include, (i) it allows for a device of a large length to readily used, since $E \propto L$, and the manufacture of long lengths of bulk material in ceramic, polymer or single crystal form can be challenging, (ii) it avoids excessively large voltages being generated during pressure ripple harvesting, since $V_{oc} \propto 1/n$; this can limit the potential damage of rectification or power management circuits and, (iii) it provides a high device capacitance and therefore a low electrical impedance ($Z = 1/j\omega C_{eq}$), since $C_{eq} \propto n^2$, which benefits impedance matching with electrical circuits.

It is of interest to also consider the conversion of mechanical strain energy to electric energy, where Uchino[57] has provided a detailed analysis in relation to the efficiency of energy harvesting using piezoelectric materials. One approach is to consider the coupling coefficient (k), which is defined as,

$$k^2 = \frac{electric \quad energy \quad stored}{mechanical \quad energy \quad applied} \tag{14}$$

In this case the electric energy stored (E) in a single cycle is given by **Equation (11)**, and the applied mechanical energy is the strain energy, namely the area under the stress-strain curve. On re-arranging **Equation (11)** to applied stress, rather than force;

$$k^2 = \frac{\frac{1}{2}\frac{d_{33}^2}{\varepsilon_{33}^T \varepsilon_0}\sigma^2 L A_s}{\frac{1}{2}\frac{\sigma^2}{1/s_{33}^E}} = \frac{d_{33}^2}{\varepsilon_{33}^T \varepsilon_0 s_{33}^E} \tag{15}$$

where s_{33}^E is the elastic compliance in the polarisation direction. Typical values of coupling coefficient are included in Table 1, which show relatively large values of k^2, typically $k^2 \sim 0.5$ - 0.8 for ferroelectric ceramics and crystals. The reader can refer to the detailed analysis provided by Uchino, [57] who highlighted that since the elastic compliance of a piezoelectric can change significantly with the electrical constraint conditions and electric impedance, the applied strain energy can also change. As a result, the energy *transmission coefficient* can also be considered to assess the overall efficiency of the system, which are described in more detail in [57,58].

Until now, we have treated the selection of piezoelectric material, and device geometry as independent design variables. Of particular interest in this regard is the maximum operating stress ($\sigma_{\max} = F_{ripple} / A_s$) of the material being used, since it places a limit on the area when harvesting a known ripple load. As indicated by Xu *et al.* [36], the generated electric field in the device must be lower than the maximum load that can be applied to the piezoelectric material without damage; this can be based on the failure or fatigue strength of the material (σ_f), or its coercive stress (σ_{coercive}) which is a compressive stress that can lead to depolarization of the material due to domain switching,

$$F_{\max} \leq \sigma_{\max} A_s \tag{16}$$

We now consider a condition where there is a specific maximum ripple force to be harvested and we wish to avoid mechanical failure of the device due to compressive failure, fatigue or depolarization of the material. If the area of the device is a variable, which is determined by $\sigma_{\max}$, substitution of **Equation (16)** into **Equation (11)** to eliminate the variable A_s leads to

$$E_{\max} = \frac{1}{2} \frac{\sigma_{\max} d_{33}^2}{\varepsilon_{33}^T \varepsilon_0} F_{\max} L \tag{17}$$

Therefore, for a fixed maximum ripple force F_{max} and a fixed device L, the properties of the material that maximize the energy can be defined by the *ripple figure of merit*, which is defined as

$$FoM_{\text{ripple}} = \frac{\sigma_{\max} d_{33}^2}{\varepsilon_{33}^T \varepsilon_0} \tag{18}$$

This figure of merit is of interest as it takes into account the harvesting capability of the piezoelectric material (**Equation (12)**), and the resistance of the material to mechanical loads (**Equation (16)**). Xu *et al.* [36] also indicated that the generated electric field (V_{oc} / t) device must always be lower than the coercive electric field of the piezoelectric to prevent depolarization; however, since the charge is often being harvested as it flows through a load resistance or is being accumulated in a storage capacitor, it can be assumed that the device is rarely under true open-circuit conditions.

In an approach analogous to that developed by van den Ende *et al.* [59], the maximum energy density (U_{max}, J m^{-3}) can also be considered by combining **Equation (11)** and **(16)**, so that

$$U_{\max} = \frac{1}{2}\frac{\sigma_{\max}^2 d_{33}^2}{\varepsilon_{33}^T \varepsilon_0} \tag{19}$$

To date, many of the multi-layer devices used for energy harvesting applications have been based on relatively 'soft' lead zirconate titanate (PZT) ferroelectric materials, which exhibit high piezoelectric d_{33} coefficients.[26,27] This is because such devices are typically manufactured as high displacement and low operating voltage multi-layer *actuators*, and not as an energy harvesting element. The soft ferroelectric materials, such as PZT-5H, exhibit high d_{33} coefficients, as seen in **Table 1**, since ferroelectric domains are relatively mobile under stress or applied electric field. The disadvantage of a soft ferroelectric is that the high domain mobility of the material (i) limits the stress levels that the material can sustain without depolarization and (ii) increases the permittivity of the material and reduces the figures of merit, **Equation (12)** and **(18)**. Since there is clearly a complex balance between the piezoelectric properties (d_{33}), dielectric properties (ε_{33}^T and tanδ) and mechanical properties ($\sigma_{\max}$), it would be of interest to conduct further studies to select the optimum combination of material and device geometry. As an example, while 'hard' lead zirconate titanate ceramics exhibit relatively low piezoelectric d_{ij} coefficients, as seen by PZT4 in **Table 1**, they also have a higher failure strength, higher coercive stress, and lower permittivity.

The maximum temperature that the harvester will experience also needs to be considered. In this regard, the Curie temperature (T_c) provides an indicator of the maximum temperature of operation since it represents the temperature of a transition from a ferroelectric phase to a paraelectric phase; at temperatures above the T_c all piezoelectric properties are therefore lost. Typically, manufacturers recommended an upper operating temperature of half of the Curie temperature (in °C). For example, soft PZT with a Curie temperature of 180 °C can be operated at up to 90 °C; although in many cases, hydraulic systems have coolers to maintain a minimum temperature. For high-temperature operation, a variety of high T_c materials are available.[60] While single crystal relaxor materials exhibit very high piezoelectric d_{33} coefficients (see **Table 1**), they can experience a rhombohedral-to-tetragonal phase transition at a temperature (T_{rt}), which is lower than the Curie temperature and can limit the operational temperature limit.

Table 1 presents data for a range of materials, which indicates the piezoelectric charge coefficient (d_{33}), dielectric properties (ε_{33}^{T}, tanδ), the piezoelectric voltage coefficient (g_{33}) and Curie temperature. The harvesting figures of merit FoM_{33} (**Equation (12)** and **(13)**), the ripple figure of merit FoM_{ripple} which include the upper-stress limit (**Equation (18)**) and maximum energy density (U_{max}, **Equation (19)**) are also calculated. Materials such as AlN, ZnO and $LiNbO_3$ have not been included since they are mainly used in thin-film form, so that large lengths are not possible. The low piezoelectric d_{33} charge coefficients of these materials also leads to a relatively low FoM_{33} harvesting figure of merit; despite their low permittivity.

Materials in **Table 1** that have been used in ripple harvesting have been identified; this includes soft lead zirconate titanate (PZT-5H[26,27,39,44], PZT-5A[55]) used in multi-layer form since multi-layer actuators are commercially available and single-crystal materials (PMN-PT[28,29]). Additional materials have been included for reference. It can be seen that the soft PZT polycrystalline ceramics, such as PZT-5H, exhibit high FoM_{33} harvesting figures of merit compared to hard PZT (PZT4) due to the high d_{33} coefficient. The introduction of dielectric loss (tanδ) leads to relatively small changes in the ranking of the materials (**Equation (9)**), since most of the materials are relatively good dielectrics of low conductivity. It can be seen that the hard ferroelectric materials exhibit a higher coercive stress, since domain motion is restricted, and these materials provide potential for smaller device areas to deliver higher power; see **Equation (11)**. This is reflected in the high ripple figure of merit (FoM_{ripple}) of the hard PZT4 in **Table 1**; which is 2.5 times higher than the soft PZT-5H ceramic - the hard material also exhibits a much higher U_{max} maximum energy density for the same reason. The single-crystal materials, such as lead magnesium niobate-lead titanate (PMN-PT) and lead indium niobate-lead magnesium niobate-lead titanate (PIN-PMN-PT), have the potential to provide harvesting figures of merit that are orders of magnitude higher than their polycrystalline materials; the disadvantage is their high cost, limited geometries, low T_c and T_{rt} temperature; these materials often exhibit low coercive stress and coercive fields, although data on such materials is often limited and are worthy of further study. For example, Skow[45] examined the potential of using phase transformation during mechanical loading to increase the power output. Domain motion and phase transformations can lead to

nonlinear dielectric, elastic and piezoelectric relationships, especially when the materials are used under extreme operating conditions, such as high stress; for more information on this topic the reader is referred to a review by Hall [66].

Efforts have been made to improve the efficiency and power generated during the energy harvesting cycle. Skow[45] examined the potential of using the high forces generated by ripples to induce a crystal phase transition in piezoelectric single crystals at hundreds of Hertz. In this regard, Dong *et al.*[67] used phase transformations to obtain a *giant* mechanical to electrical energy conversion, where the phase-transition of a ferroelectric crystal resulted in an output electrical energy density per cycle, which was almost two orders of magnitude greater than the energy density per cycle for linear piezoelectric materials. Vats *et al.*[68] explored a novel approach for electro-mechanical energy conversion by combining the alternating mechanical stress with an applied cyclic electric field in ferro-electric materials; this approach is analogous to a similar concept developed by Olsen and Evans[69] to harvest thermal fluctuations using ferroelectric materials. In this case, the energy density improved by two orders of magnitude compared to the conventional linear piezoelectric effect. It would be of interest to explore either phase changes or combined mechanical and electrical loading to enhance the efficiency of energy harvesting pressure ripples.

Table 1 Properties of piezoelectric materials. Materials include lead zirconate titanate (PZT), lead magnesium niobate-lead titanate (PMN-PT) and lead indium niobate-lead magnesium niobate-lead titanate (PIN-PMN-PT) at the morphotropic phase boundary (MPB).

Materials	**PZT 5H (soft type)**	**PZT 5A (soft type)**	**PZT 4 (hard type)**	**TRSX2B PMN-PT**	**PIN-PMN-PT (MPB)**
d_{33} [pC N^{-1}]	593 (Ref [3])	374 (Ref [3])	289 (Ref [3])	1860 (Ref [45])	2740 (Ref [63])
Relative permittivity at constant stress, (ε_{33}^{T})	3400 (Ref [61])	1700 (Ref [61])	1300 (Ref [61])	5000 (Ref [62])	7240 (Ref [63])
g_{33} [10^{-3}Vm N^{-1}]	19.7	24.8	26.1	42.0	42.8
Curie Temperature (T_c) or T_{rt} [°C]	T_c =193 (Ref [61])	T_c =365 (Ref [61])	T_c =328 (Ref [61])	T_{rt} = 85-98 T_c > 142 (Ref [62])	T_c = 197 T_{rt} = 96 (Ref [63])
Dielectric loss (tanδ)	0.02 (Ref [61])	0.02 (Ref [61])	0.004 (Ref [61])	≤0.006 (Ref [62])	--

Coercive stress [MPa]	20 (Ref [64])	20 (Ref [61])	82 (Ref [61])	--	--
Coercive field [kVcm^{-1}]	5.5 (Ref [65])	11.8 (Ref [65])	14.4 (Ref [65])	1.9-2.5 (Ref [62])	5.5 (Ref [63])
FoM_{33} (Equation (12)) [10^{-12} m^2 N^{-1}]	11.69	9.35	7.26	78.18	117.17
FoM_{33} / tanδ (Equation (13)) [10^{-14} m^2 N^{-1}]	5.84	4.65	18.15	130.31	--
FoM_{ripple} (Equation (18)) (10^{10})	2.34	1.86	5.95	--	--
U_{max} [Jm^{-3}]	2337	1859	24406	--	--
k_{33}^2 coupling coefficient	0.56 [61]	0.50 [61]	0.49 [61]	0.83-0.90 [62]	0.90 [63]
Used for ripple harvesting	✓ (Ref [26,27,39,44])	✓ (Ref [55])	×	✓ (Ref [28,29])	×

In addition to piezoelectric materials, the potential of using magnetostrictive materials for hydraulic ripple harvesting has been discussed, [47] but has yet to be examined in detail in the literature. While piezoelectric materials change polarisation with stress, magnetostrictive materials can induce a current into a coil as a result of a change in magnetization with stress, as seen in **Figure 6(b)**.

While the *piezo-electric* d_{33} coefficient is a measure of the charge density per unit stress, or strain per unit electric field, the *piezo-magnetic* coefficient d_{33}* of a magnetostrictive material can be characterised by its magnetostriction (λ) versus magnetic field (H) curve, or its flux density (B) versus stress (σ) curve; [70]

$$d_{33}^{*} \equiv \frac{d\lambda}{dH} = \frac{dB}{d\sigma} \tag{20}$$

In this case the material is magnetized by an externally applied magnetic field, as indicated by the bias magnet located in the lower part of **Figure 6(b)**. Examples of magnetostrictive materials include an alloy of terbium, dysprosium and iron ($Tb_{0.3}Dy_{0.7}Fe_2$), termed Terfenol-D, and Fe-Ga alloys, termed Galfenol. There are some advantages of these materials compared to piezoelectric materials. The existence of a static magnetic field reduces the potential loss of polarisation during operation at high stress, unlike the relatively low coercive strengths of piezoelectric materials. In addition, the higher compressive strength of the materials provides an opportunity to operate at a higher stress, compared to brittle

piezoelectric ceramics; [71,72] for example, Terfenol-D can exhibit a compressive strength in excess of 300MPa.[73] Given the high stress and power intensity associated with ripple harvesting, it would be of interest to examine the potential of magnetostrictive materials in more detail. The potential disadvantages of using such materials are the need for current collection coils and bias magnets, which can increase harvester size and complexity, and the strong non-linear properties of the materials.[72]

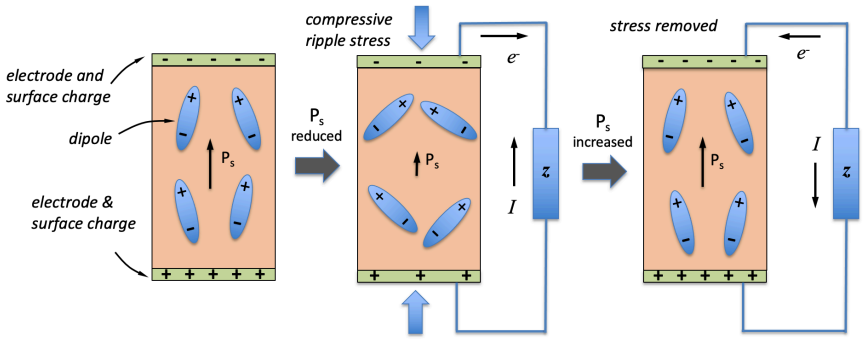

(a)

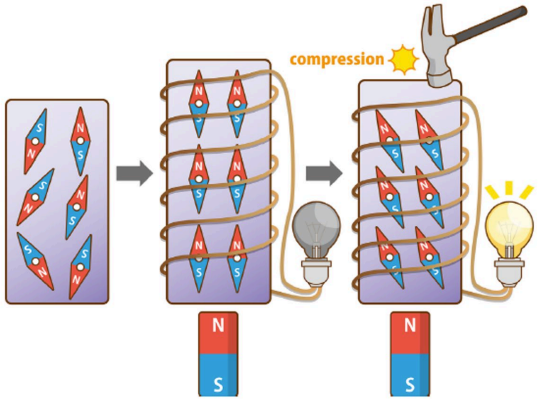

(b)

Figure 6. (a) Generation of piezoelectric charge due to a change in polarisation under a compressive or tensile stress, (b) Generation of current due to change is magnetization under stress (Villari effect). Reproduced with permission.[71] Copyright 2018, WILEY-VCH Verlag GmbH & Co.

In recent years, using triboelectric materials for energy harvesting has received increasing interests, as the raw materials are widely accessible, lightweight, mechanically flexible, and low-cost.[74-77] A triboelectric nanogenerator (TENG) exploits the triboelectric effect to convert mechanical energy into electrical energy, and is an emerging technology that has shown remarkable potential in low-frequency vibration energy harvesting and power

generation.[78-82] Triboelectric nanogenerators have four basic operation modes, which include the vertical contact-separation mode, in-plane contact-sliding mode, single-electrode mode, and freestanding triboelectric-layer mode.[74] To date, TENGs developed for acoustic wave energy collection generally operate in vertical contact-separation mode and are manufactured using flexible electrode materials due to their ease of fabrication and high voltage output, and are designed to convert acoustic wave energy into electricity using a Helmholtz resonator or quarter-wavelength resonator to generate enhanced excitation.[83-87] Materials that have been used as triboelectric films include polytetrafluoroethylene (PTFE)[83], electrospun polyvinylidene fluoride (PVDF) nanofibers[84,85], and fluorinated ethylene propylene (FEP) [86,87] due to their tendency to capture electrons from other materials and the long-time surface charge maintenance.

In the contact-separation mode, a thin membrane will alternatively contact and separate from a conductive perforated layer with the propagation of acoustic waves, and an electrical output is generated due to the coupling of triboelectric effect and electrostatic induction, as shown in **Figure 7**. The generated open-circuit voltage for a device based on a membrane can be expressed as [86,87]

$$V_{oc} = \frac{\sigma_d x(t)}{\varepsilon_0} \tag{21}$$

where V_{oc} is the open-circuit voltage, σ_d is the charge density, ε_0 is the dielectric constant, $x(t)$ is the radial displacement of the membrane. As the acoustic pressure increases, the radial displacement of the membrane increases, and a higher output is produced. A sharp increase of the generated voltage and current with the input sound pressure level (SPL) was observed. The power output was 4.33 mW under 100 dB SPL excitation, which is sufficient to directly drive low-power electronics. [87] However, the triboelectric materials and devices have yet been examined for hydraulic ripple harvesting with a much higher power intensity compared to acoustic wave. It would therefore be of interest to explore the potential of triboelectric materials and devices for high power intensity hydraulic ripple harvesting, including hybrid systems that aim to combine triboelectric effects with additional mechanisms such as piezoelectric or electromagnetic.

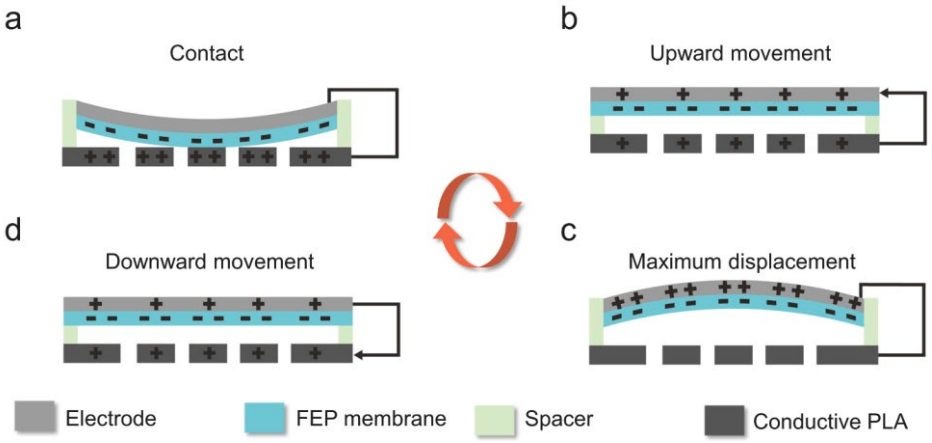

Figure 7. Working mechanism of TENG device in contact-separation behavior for acoustic wave harvesting. Reproduced with permission.[87] Copyright 2021, Elsevier Ltd.

4. Novel directions for performance improvement

4.1 Acoustic resonators

Generally, for a hydraulic pressure energy harvester employing a mechanical-to-electrical transducer, such as a piezoelectric or magnetostrictive material, the output power is a function of the pressure amplitude and area of the interface; see **Equation (4)** and **(11)**. As a result, power generation for a given HPEH can increase either by (a) increasing the area of the fluid to the mechanical interface, and hence the force acting on the transducer; or (b) improving the electro-mechanical properties or geometry of the transducer. For hydraulic systems where an area increase in the fluid to mechanical interface is not practical, for example, due to size constraints or potential to compromise the mechanical integrity of the fluid to mechanical interface, researchers have proposed the use of acoustic resonators as an alternate force amplification mechanism.

An acoustic resonator is an acoustic device that consists of a cavity coupled to a fluid medium via a neck, or a port connection to the fluid flow, as shown in **Figure 8**. As described in Section 2, within hydraulic systems the dominant frequency of the pressure ripple is typically a harmonic of the pump operating frequency and in the range of hundreds of Hz. In contrast, the resonance frequency of a piezoelectric stack is typically in the kHz range and is therefore much higher than the dominant pressure frequencies. As a result, the hydraulic pressure energy harvesters are usually *non-resonant* energy harvesting systems. The primary function

of an acoustic resonator for hydraulic pressure energy harvesting is to amplify the amplitude of the pressure ripples when the dominant frequency of the ripple is within the bandwidth of its resonance, thereby increasing the force generated by the fluid to mechanical interface; such systems are therefore *resonance*-based.

Acoustic resonators have been widely used in conventional hydraulic systems as narrowband attenuators.[88-90] In the area of energy harvesting, the acoustic properties of these devices have been exploited to increase the amplitude of pressure waves inside the device cavity, and thereby improve power generation.[91] The majority of studies investigating acoustic resonators are designed for media of low density, such as noise suppressors and accumulators with air as a medium.[91-93] For such acoustic resonators, the incident sound power density is relatively low. The power intensity of acoustic noise is 0.003 μW cm^{-2} at sound pressure level of 75 dB and 0.11 μW cm^{-2} at sound pressure level of 110 dB.[24] Acoustic resonators are able to amplify the incident acoustic wave and excite energy conversion component. For hydraulic fluid system that use a higher density fluid medium, the power intensity can be up to 45 W cm^{-2} for a pressure ripple amplitude of 1 MPa and 547 W cm^{-2} for pressure ripple amplitude of 3.5 MPa, as described in Section 2. Although the power intensity of the ripple is high, the energy harvesting performance of the HPEH is limited due to the *non-resonant* of the hydraulic pressure energy harvesters. Therefore, acoustic resonators have also been introduced to amplify pressure fluctuations at given frequencies and to improve the energy harvesting capabilities of HPEH. However, only a limited number of studies have been reported to date. Skow *et al.*[94] proposed to use a Helmholtz resonator to improve the hydraulic pressure energy harvesting performance of a system with pressure ripples at 250, 450, 600, and 900 Hz. The authors predicted up to 7 dB power gain when the dominant pressure ripple frequency coincided with the resonant frequency of the device. The study revealed that the acoustic performance is significantly affected by viscosity, air content inside the hydraulic fluid, and viscous losses in the neck. A major challenge for the employment of a Helmholtz resonator in high-density fluids is the impractical size of the resonator to operate at low resonant frequencies. This problem arises from the cavity volume or narrow neck diameters needed to achieve relatively low resonant frequencies (<1kHz). For example,

assuming a classical Helmholtz resonator (**Figure 8(a)**), where the size of the device is smaller than the wavelength of the pressure ripples, the resonant frequency can be calculated as follows[94]

$$f_{res} = \frac{1}{2\pi}\sqrt{\frac{A_{neck}c_f^2}{l_{n,eff}V_{cavity}}} \tag{22}$$

where f_{res} is the frequency in Hz, c_f is the speed of sound characteristic of the fluid, $l_{n,eff}$ is the effective neck length and V_{cavity} is the volume of the cavity. A reduction in the resonant frequency of a classical Helmholtz resonator requires either a decrease in the diameter of the neck, an increase in the length of the neck, or an increase in the volume of the cavity.[94] Reducing the neck diameter also impacts the acoustic performance since narrow necks can lead to a reduction in acoustic gain due to viscous losses. On the other hand, increasing the size of the device could be impractical for some energy harvesting applications when volumetric constraints exist. Approaches to solving the challenges in the design of compact Helmholtz resonators include the use of foam liners,[95] where lining the inside of the Helmholtz resonator cavity can lead to a lower resonant frequency in noise reduction applications. However, this has yet to be demonstrated for energy harvesting purposes.

Aranda *et al.*[48] demonstrated that a space-coiling resonator, an alternative to the classical Helmholtz resonator, as seen in **Figure 8(b)**, can achieve a better acoustic gain than the Helmholtz resonator bounded by the same volume. The advantage of the space-coiling resonator is its longer and wider neck, which can be accommodated in a small volume by coiling the neck. The structure was fabricated in nylon using 3D printing techniques (HP Multi-jet fusion). The space-coiling resonator experimentally exhibited a better acoustic gain compared to a Helmholtz resonator of the same volume mainly at the low resonant frequency of around 300 Hz which can significantly increase the power generated by an HPEH, which was measured to be 15 mW bar^{-2} at 920 Hz and 1.2 mW bar^{-2} at 280 Hz.

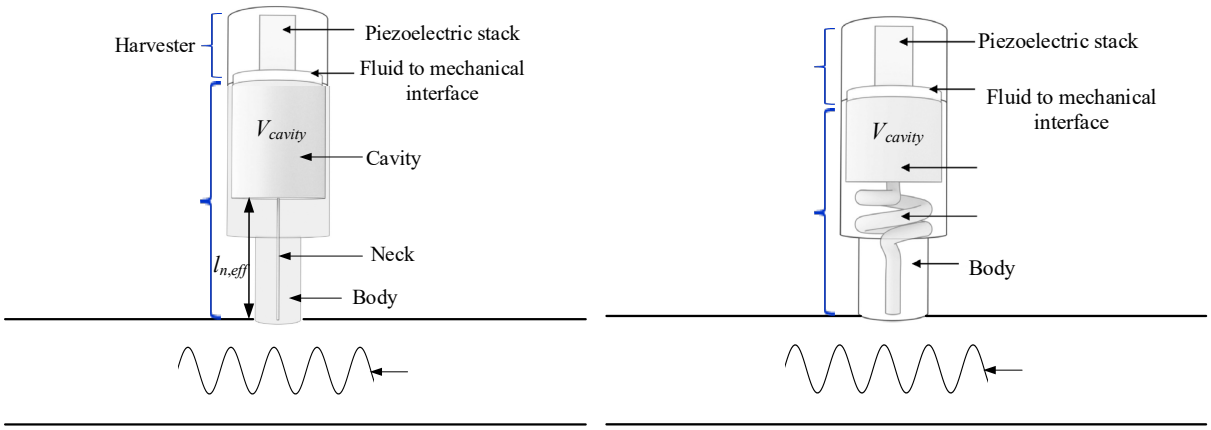

Figure 8. (a) Hydraulic pressure energy harvester coupled to a Helmholtz resonator and (b) Hydraulic pressure energy harvester coupled to a space-coiling-resonator. Adapted with permission.[48] Copyright 2019, Elsevier B.V.

The major challenges for acoustic resonators in hydraulic pressure energy harvesting are the optimization of acoustic gain, especially at low resonant frequencies and a broadening of the amplification range. An acoustic resonator for hydraulic pressure harvesting acts as a low pass filter, [91] which means that pressure ripples with frequencies higher than the natural frequency of the resonator are attenuated. Furthermore, as discussed in,[48,91] the air content of the fluid, temperature, and compliance of the materials can significantly change the acoustic behavior of the resonator, which has to be taken into consideration in the design of the hydraulic pressure energy harvesting.

4.2 Force amplification

We have seen from **Equation (4)** and **(11)** that increasing the force applied to the electro-active material can increase the power. As a result, piezoelectric stack energy harvesters (PSEHs) that exploit a force amplification frame have been explored. This form of harvester design has been widely studied for low-frequency compressive force energy harvesting [96-99] due to the high electrical power output as a result of the force amplification mechanism and the high electro-mechanical performance of the piezoelectric stacks used. [100]

A schematic of a piezoelectric stack energy harvester with a force amplification frame is

shown in **Figure 9(a)**. Such a design consists of a piezoelectric stack and a mechanical force amplification frame. The inclined beams of the mechanical frame have a tilted angle β and both ends of each inclined beam serve as flexure hinges. To simplify the analysis, it is assumed that the hinges are free to flex, while the inclined beams do not change their lengths. In a quasi-static state, the following relationships can be obtained for the force and displacement[98, 101]

$$F_z = F_x \cot\beta, \quad D_x = D_z \cot\beta \tag{23}$$

where F_x and D_x are the input force and displacement; F_z and D_z are the force and displacement of the piezoelectric stack.

Equation (23) suggests that when β is small, the mechanical frame amplifies F_x by a factor of cotβ. It is this force amplification mechanism that attracts wide interests from the energy harvesting research community because the electric power output of a PSEH increases proportionally with the square of the cotβ and can be ten-hundredfold; see **Equation (11)**. **Equation (23)** also indicates that while amplifying the force, the mechanical force amplification transformer reduces the displacement D_x by a factor of cotβ. This leads to the stiffness along the x-axis (k_x) being lower than that along z-axis (k_z) since

$$k_x = \frac{F_x}{D_x} = \frac{1}{\cot^2\beta} \cdot \frac{F_z}{D_z} = \frac{k_z}{\cot^2\beta} \tag{24}$$

Piezoelectric stacks have high stiffness, leading to a resonance frequency usually in the range of tens of kilohertz, in contrast to the usual low frequencies of fundamental pressure ripples of tens to hundreds of hertz. The reduction in the stiffness can lower the resonance frequency of the piezoelectric stack energy harvester to match the ambient vibration to create a resonant device. While **Equation (24)** can be used for qualitative analysis, it must be noted that, in reality, the relationship between the force/displacement amplification and the tilted angle is more complex due to the elastic deformation of the inclined beams.[98,99,101]

Piezoelectric stack energy harvesters specifically designed for vibration energy harvesting have been studied [102,103] and are shown in **Figure 9(b)-(d)**. A notch hinge design was used for the inclined beams, where the thickness of the flexure hinges was much smaller than the

middle section of the inclined beam. This device architecture allows easy bending of the hinges, while reducing the elastic deformation and energy storage in the inclined beams.

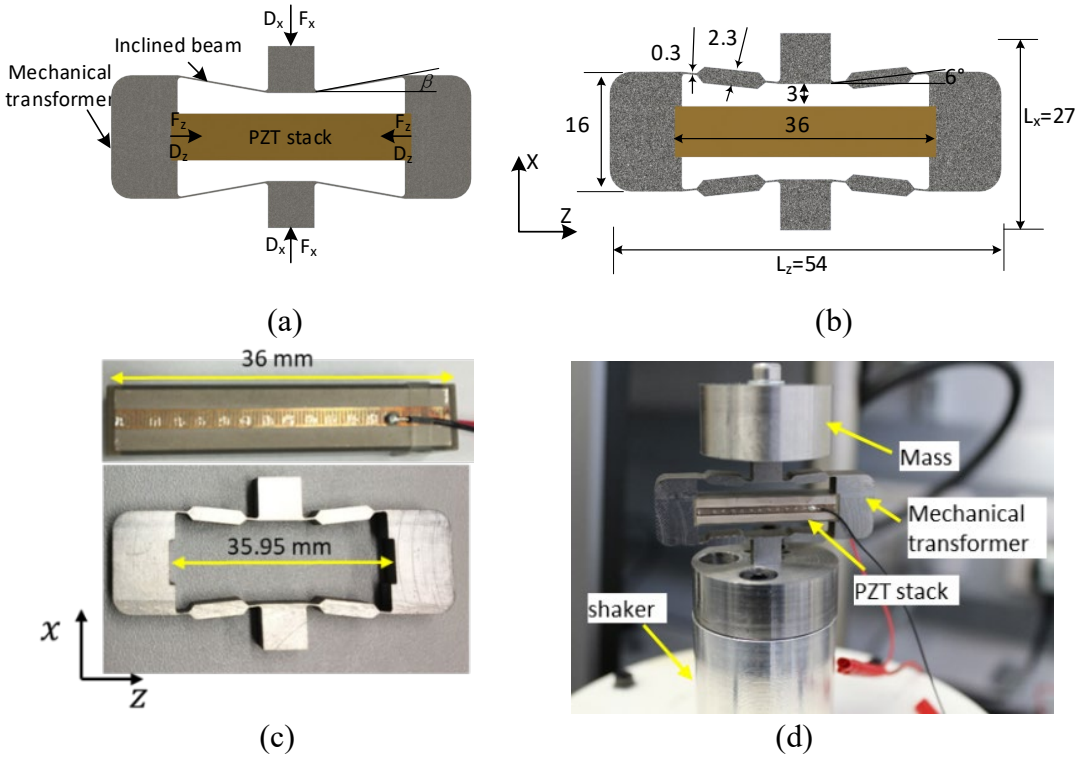

Figure 9. (a) Operating principle of a piezoelectric stack energy harvester with mechanical force amplification, (b) Piezoelectric stack energy harvester (PSEH) design with a mechanical force amplifier: units in mm unless specified, (c) Fabricated mechanical transformer and multi-layer PZT stack used for the piezoelectric energy harvester, and (d) Fully assembled piezoelectric stack energy harvester installed on a shaker for testing. Reproduced with permission.[103] Copyright 2020, Elsevier Ltd.

Piezoelectric stack energy harvesters with a force amplification frame can be used to harvest fluid ripple energy and **Figure 4 (d)** shows a potential design that uses the force amplification frame.[44] *Force amplification* acts to increase the force on the transducer cotβ times (cotβ = 4-10) and increase the energy harvested cot$^2\beta$ times (16 to 100 fold for cotβ = 4-10) and allow operation at the non-resonant frequency with a high power output over a range of operational frequencies; the low resonant frequency of the frame also provides a potential for resonant operation. Such configurations are well known in piezoelectric actuator designs; however, they have yet to be fully explored for hydraulic pressure harvesting. One can expect the transducer configuration to outperform current transducers that directly use a piezoelectric

stack by providing 10 to 100-fold in power output, if the transducer is optimized to withstand the fluid pressure.

4.3 Acoustic metamaterials

Generally, the fundamental frequency components of pressure ripples are relatively low, namely in the range of hundreds of hertz[4,45,104], which is typically well below the fundamental resonance frequency of a piezoelectric element, which is often in the order of tens of kHz. The architectures of acoustic resonators are designed to lower the resonance frequency and improve the energy harvesting efficiency in pressurized fluid applications, as presented in Section 4.1.

As an alternative approach, *acoustic metamaterials* have recently shown significant potential for low-frequency acoustic absorption and energy harvesting. Acoustic metamaterials are engineered materials that exhibit unusual constitutive parameters which are usually constructed from local resonance of subwavelength structures and can control acoustic waves by creating an artificial periodic geometry formed from conventional materials, such as metals and polymers[4,105-107], as shown in **Figure 10**. It is possible to decrease the size of the complete harvesting device for low-frequency energy harvesting since the local resonant frequency of metamaterials usually depends on both the geometrical arrangement and material properties, rather than simply on the dimension of the structure.[4]

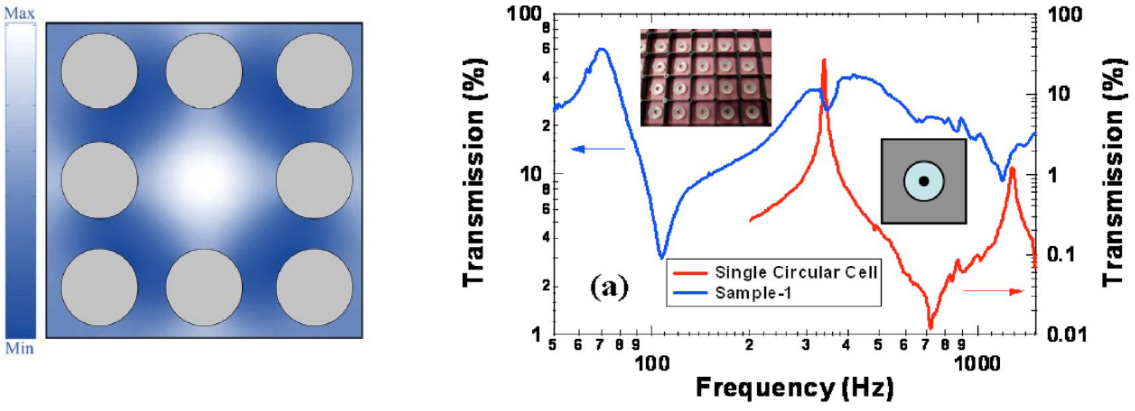

(a) (b)

Figure 10. (a) Pressure distribution of the acoustic metamaterial at the defect mode. Reproduced with permission.[4] Copyright 2019, Elsevier Ltd. (b) Transmission spectra of a

single circular cell (red) and the 2D array of unit cells (blue). Reproduced with permission.[106] Copyright 2010, American Institute of Physics.

While acoustic metamaterials are currently widely used for low-frequency acoustic absorption or energy harvesting, there is potential for innovations in these new materials to be exploited in harvesting the significant energy from pressure ripples in hydraulic systems; this is due to its similar characteristics in terms of being a low-frequency energy source. As a result, current research on acoustic metamaterial in low-frequency acoustic energy harvesting is presented to inspire potential new directions in pressure ripple harvesting.

Liu *et al*. [107] firstly presented the concept of an *acoustic metamaterial*, also termed a *localized resonant structure*. For low-frequency energy harvesting applications, Yuan *et al.*[108] proposed an *acoustic metastructure* to achieve low-frequency sound isolation and acoustic energy harvesting. The acoustic metastructure was composed of a metallic substrate, a piezoelectric patch and a proof mass, as shown in **Figure 11(a)**. The harvested power of the proposed metastructure was 0.21 mW at 155 Hz under 114 dB sound pressure excitation. Sun *et al*.[109] proposed an acoustic energy harvester that used a doubly coiled-up acoustic metamaterial cavity with an embedded piezoelectric bimorph plate to harvest low-frequency acoustic waves, as shown in **Figure 11(b)**. The acoustic pressure was amplified in an acoustic metamaterial cavity to induce mechanical vibrations of a piezoelectric plate to generate electrical energy. The resonance frequency matching between the acoustic metamaterial cavity and the piezoelectric plate led to a relatively low maximum output power of 0.345 μW at 600 Hz for an incident sound pressure level of 100 dB. A membrane-type acoustic metamaterial based on the principle of local resonances exhibited advantages of being lightweight and compact in construction and has been used for low-frequency acoustic energy harvesting. Wang *et al.* [110] proposed a compact acoustic energy harvester that consisted of a beam-based lead zirconate titanate (PZT) transducer and a dual-layered membrane-type acoustic metamaterial to harvest low-frequency sound energy, as shown in **Figure 11(c)**. A similar resonant frequency matching approach was exploited for the design of a PZT transducer to achieve maximum pressure amplification. The proposed energy harvesting

system was able to enhance the sound pressure level by 18 dB at 318 Hz. Li *et al.* [111] attached a polyvinylidene difluoride (PVDF) piezoelectric polymer thin film on both sides of a circular thermoplastic polyurethane (TPU) membrane-type acoustic metamaterial to convert acoustic energy into electric energy at a resonant frequency of 356 Hz, as shown in **Figure 11(d)**. However, the power of the harvested energy is in the order of nW due to the relatively low electromechanical properties of the PVDF materials and its small volume. Gao *et al.*[112] designed a radial membrane acoustic metamaterial structure in which the membrane was covered with a multi-layer of rigid ring materials, as shown in **Figure 11(e)**. A multiple low-frequency band gap behavior in the metamaterial was observed, where in these frequency ranges the propagation of acoustic waves was restrained. This unique characteristic in the low-frequency acoustic absorption demonstrates significant potential for pressure ripple harvesting in the broadband low-frequency range.

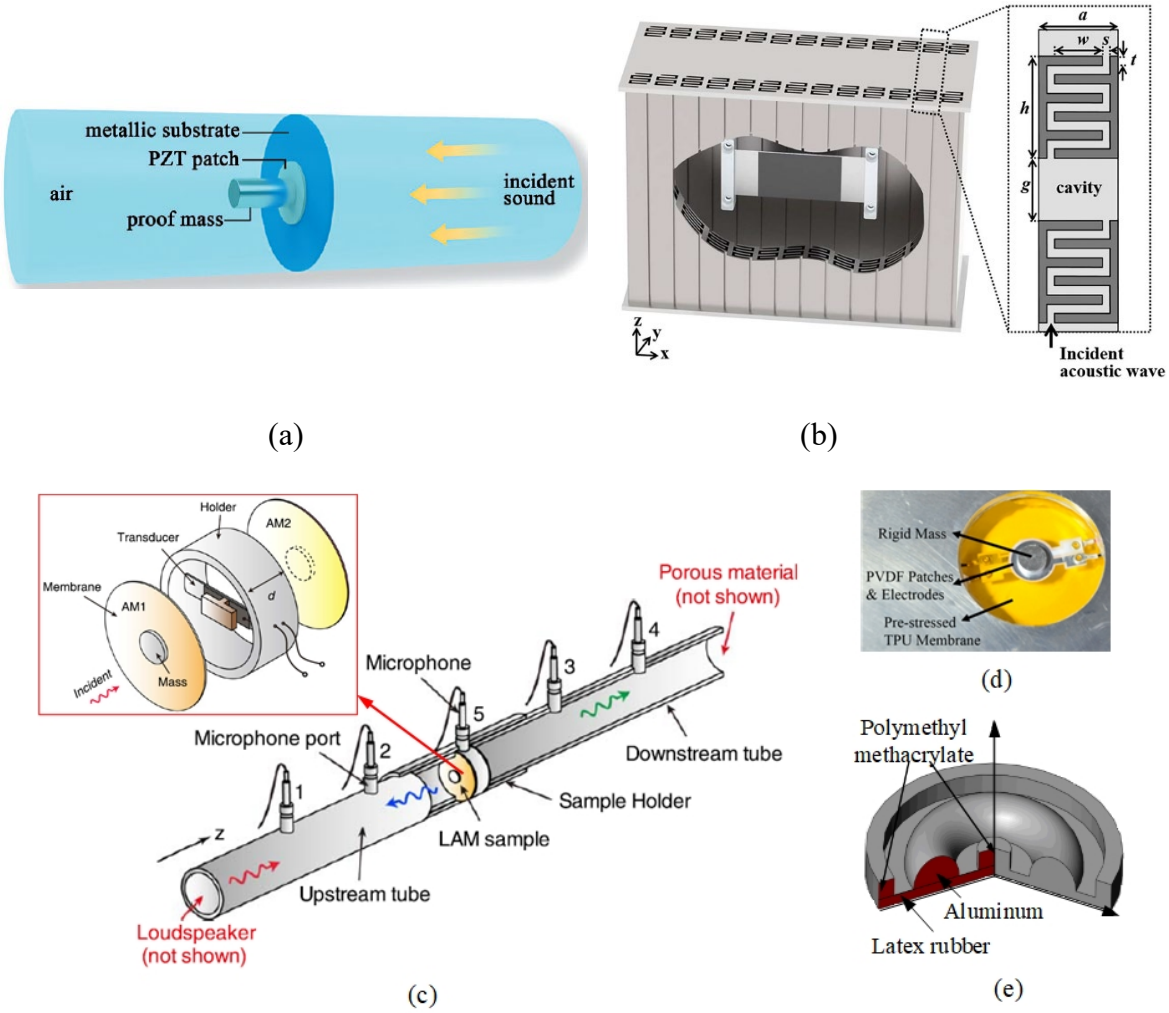

Figure 11. Range of *acoustic metamaterial* structures (a) A metallic substrate, a piezoelectric patch and a proof mass. Reproduced under the terms of the CC-BY license.[108]

Copyright 2018, The Authors. (b) Double-clamped piezoelectric bimorph plate. Reproduced with permission.[109] Copyright 2017, IOP Publishing Ltd. (c)Beam-based lead zirconate titanate (PZT) transducer and a dual-layered membrane-type acoustic metamaterial. Adapted with permission.[110] Copyright 2019, IOP Publishing Ltd. (d) Circular thermoplastic polyurethane (TPU) membrane-type. Reproduced under the terms of the CC-BY license. [111] Copyright 2016, IOP Publishing Ltd. (e) Radial membrane acoustic metamaterial structure in which the membrane was covered with a multi-layer of rigid ring materials.[112] Copyright 2016, World Scientific Publishing Company.

It should be highlighted that current acoustic metamaterials and structures are designed to operate with acoustic signals in a lower density air medium. It remains a challenge for acoustic metamaterial concepts to be transferred to harvesting pressure ripples in hydraulic systems using higher density fluid mediums. The challenges are associated with the lower speed of sound and lower resonant frequency for fluid mediums, as illustrated by **Equation (22)**. The geometrical arrangement and materials have to accommodate the lower resonant frequencies from air medium to fluid mediums with the given volumetric constraint. In addition, the metamaterials and structures must be able to endure the higher static and dynamic pressures in hydraulic systems.

5. Performance comparison and applications

We now summarize the range of conditions and power levels reported to date for energy harvesting of pressure ripple, as shown in **Table 2**, which include testing using hydraulic systems and shaker systems aiming to replicate the pressure ripples. The maximum output power for different hydraulic pressure harvesters is in the level of tens of μW to hundreds of mW, depending on the geometry and piezoelectric material of hydraulic pressure energy harvesting (HPEH) device, excitation frequency and applied force. This is in agreement with **Equation (11)** where large forces, high frequencies, long piezoelectric element lengths and good electro-mechanical properties are beneficial. The output power can be potentially increased through the optimization of the hydraulic pressure harvesting devices with the purpose to increase the compressive force applied to the piezoelectric material. For example, a

hydraulic pressure energy harvester can generate a power of 10mW under a force with an amplitude of 56.57 N at a frequency 200 Hz,[37] and a device configuration with a force amplification frame can generate power up to 29 mW under an alternating force with an amplitude of 100 N at 100 Hz on a longer stack.[38] In hydraulic systems, the amplitude of pressure ripple can reach up to 35 bar (3.5 MPa),[33] the corresponding power intensity is 547 W cm^{-2} for a hydraulic fluid density of 800 kg m^{-3} and speed of sound of 1400 m s^{-1}; therefore, the potential to harvest energy from the high-intensity pressure fluctuations shows promising prospect by optimization of the materials and device configuration.

Table 2 Summary of the harvested energy, and operating conditions in pressure ripple energy harvesting studies.

Reference	Piezoelectric material	Structure	Device capacitance (nF)	Peak force (N)	Pressure (bar)	Frequency (Hz)	Power (mW)	Power/bar. volume stack (μW $bar^{-1}mm^{-3}$)	Origin of load
Cunefare *et al.* [26]	Nd-doped PZT (6.8×6.8×30mm)	PZT stack	3060	4.45	0.768	450	0.15	0.14	Hydraulic system
				8.32	1.434	450	0.52	0.26	
			3110	7.6	0.834	450	0.38	0.33	
				14.1	1.547	450	1.23	0.57	
Skow *et al.* [113]	Nd-doped PZT (6.8×6.8×30 mm)	PZT stack	3080	8.63	1.059	450	0.90	0.61	Hydraulic system
				9.81	1.205	450	2.18	1.31	
Verma *et al.* [27]	Piezoelectric chip (5×5×2mm)	Piezoelectric chip	1560	26.1	2.961	450	0.14	0.97	Hydraulic system
				49.2	5.576	450	0.16	0.57	
Skow *et al.* [29]	Single crystal stack (5×5×11.76mm)	Single crystal stack	38	3.5	0.141	200	0.15	3.64	Hydraulic system
				5.94	0.948	450	0.52	1.86	
Skow *et al.* [28]	PZT 5A (6.8×6.8×30 mm)	PZT stack	3080	9.44	1.160	450	1	0.62	Hydraulic system
	PZT 5A (6.8×6.8×30 mm)	PZT stack	3080	15.2	1.865	450	2	0.77	
	Piezoelectric chip (5×5×2mm)	Piezoelectric chip	1417	10.33	1.171	450	0.05	0.85	
	single crystal stack (5×5×11.76mm)	Single crystal stack	42	11.83	1.341	450	1.2	3.04	
Aranda *et al.* [47]	PZT Navy V (5×5×9 mm)	PZT stack	750	7.85	1	100	0.01	0.05	Hydraulic system
					1	500	0.003	0.15	
Xiao *et al.* [55]	PZT-5A (5×5×18 mm)	PZT stack	780	0.36	0.003	10	0.003	0.05	Shaker
				2.02	0.016	10	0.007	0.02	

Aranda *et al.* [114]	ThorLabs PK4FYP2 (5×3×36mm)	HR with spiral neck	3500	--	0.8	200	2.40	5.56	Hydraulic system
Xu *et al.* [37]	PZT Navy II (7.1×7.6×32.4 mm)	PZT stack	2500	14.14	2.886	700	2	0.47	Shaker
				56.57	11.545	200	10	0.58	
Qian *et al.* [38]	PZT Navy II (7.1×7.6×32.4 mm)	PZT stack with force amplification	2500	100	20.408	100	29	0.95	Shaker
Liu *et al.* [115]	PZT Navy II (7×7×32 mm)	PZT stack with force amplification	2100	846	23.265	2.3	2.35	0.64	Shaker

Energy harvesting in hydraulic systems have been investigated for more than one decade and a variety of energy harvesters have been designed; we now overview the practical applications of these devices.

Hydraulic energy harvesting techniques have been applied to pipeline system with pumps and to power wireless sensors. Schwartz *et al.*[6] designed a complete hydraulic energy harvesting system, where the hydraulic pressure energy harvester (HPEH) with piezoelectric multi-layer stack as the energy conversion element was inserted into a pipe, as shown in **Figure 12(a)**. They studied the output power of the hydraulic pressure energy harvester and measured the power consumption of commercial wireless sensor systems, as well as the feasibility of energy-autonomous operation. It was shown that the output power of the hydraulic pressure energy harvesting system is 2.6 mW under a pressure fluctuation with a frequency of 450 Hz and amplitude of approximately 2 bar (~0.2 MPa).

Aranda *et al.*[50] designed a pressure pulsation generator, as shown in **Figure 12(d)**. The device was able to generate common pressure pulsations in hydraulic systems for performance estimation of hydraulic pressure energy harvesters. For example, it provided a static pressure up to 300 bar (~30 MPa), and generated a maximum pressure pulsation of 28 bar (~2.8 MPa) at 40 Hz, or a maximum pressure fluctuation of 0.5 bar (~0.05 MPa) at 1000 Hz. The device was also able to generate more complex signals from actual fluid power systems. A piezoelectric stack was used as the actuator for energy harvesting, which can withstand high compression forces caused by static pressure. More recently, they presented a full system implementation of the self-powered wireless pressure sensor, which integrated the hydraulic pressure energy harvester on the pressure pulsation generator and supplied power to the self-powered wireless pressure sensor (SP-WPS).[114] A thin metal plate was used as the fluid-to-mechanical interface to connect the piezoelectric stack to the fluid and installed between the housings, as shown in **Figure 12(b)**. The operating characteristics of the hydraulic system, including the static pressure, the amplitude of pressure ripples, force transmission ratio and generated power, were considered in the design of the interface plate. A space-coiling-resonator (SCR) was employed to improve the performance of the hydraulic

pressure energy harvester at lower frequencies without increasing the volume of the resonator, as shown in **Figure 12(b) and (c)**. It was shown that the self-powered sensor system can begin to harvest energy from pressure fluctuations with amplitude at 0.2 bar (~0.02 MPa) and a frequency of 200 Hz. The harvested energy is sufficient to provide the sampling and transmitting rate of approximately 100 Hz at 0.7 bar (~0.07 MPa) at 200 Hz.

To amplify the excitation forces acting on the piezoelectric stack and improve the energy conversion efficiency of the hydraulic pressure energy harvester during low-frequency excitation, Cao *et al.*[44] introduced a hydraulic pressure energy harvester using a force amplification frame to build a hydraulic pressure pipeline system, as shown in **Figure 12(e)**. This allowed measurement of the open-circuit voltage for HPEH structures with force amplifiers subjected to pressure fluctuations at frequencies of 47 Hz, 50 Hz and 100 Hz. The output density, which was defined as the ratio of the peak value of open-circuit voltage to the contact area, of 517 V m^{-2} was observed; whilst no power values were provided. It was also shown that the output performance of the energy harvester was significantly influenced by the geometry of the force amplifier. Therefore, the optimization of the force amplifier structure also shows attractive potential for improvement of power output over a range of operational frequencies in non-resonant conditions.

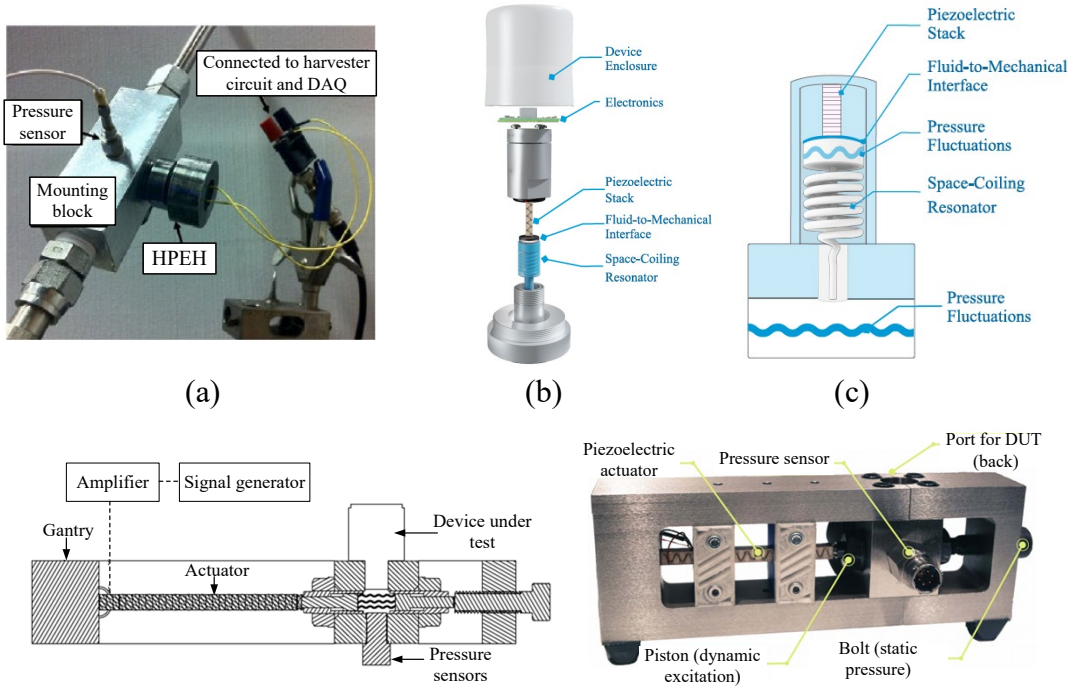

(d)

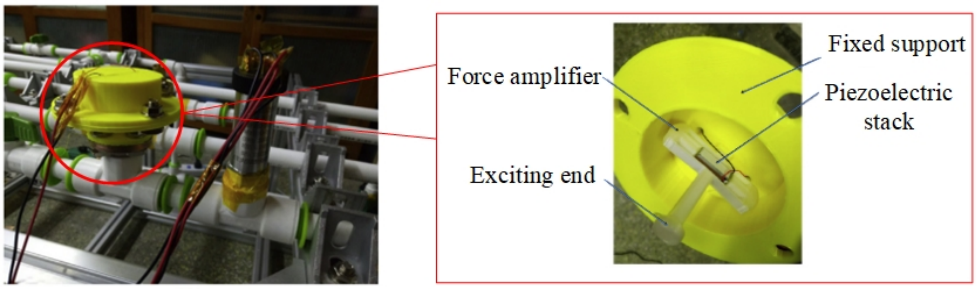

(e)

Figure 12. (a) Image of hydraulic pressure energy harvesting device mounted on a test block within a hydraulic test rig. Reproduced with permission.[6] Copyright 2017, SPIE. (b) Overview of the self-powered wireless sensor detailing the different components, (c) General principle of the pressure fluctuation energy harvester and its components. Reproduced under the terms of the CC-BY license.[114] Copyright 2021, The Authors. (d) Apparatus for the exploration of the pressure fluctuation energy harvester. Reproduced under the terms of the CC-BY license.[114] Copyright 2021, The Authors (left); Adapted with permission.[50] Copyright 2018, IEEE (right). (e) Experimental platform of the hydraulic pressure energy harvester with force amplifier. Adapted with permission.[44] Copyright 2020, Elsevier B.V.

6. Conclusions and future directions

This paper has presented a comprehensive review on the state-of-the-art techniques of hydraulic pressure energy harvesting and the associated critical aspects including the origin of pressure ripples and their power intensity, typical device configurations, the fluid-mechanical interface, the selection of electro-active materials, and applications. The inherently high power intensity of the pressure ripples makes it particularly attractive for energy harvesting. Nevertheless, while hydraulic pressure energy-harvesting has received significant interest over the last decade, which has led to a range of different designs and methods being adapted to different hydraulic environments, there remains significant potential to improve performance and implement self-powered devices. Currently, the performance in terms of power output of most hydraulic energy harvesters have been evaluated under relatively idealized conditions with a harmonic force with a deterministic frequency, based on the periodic nature of pressure ripple in hydraulic systems, e.g., a pump operating at a specific

frequency. However, for locations away from the pump or where other components are present, such as valves, the pressure ripples can be broadband or contain random disturbances. The performance of hydraulic pressure energy harvesting under broadband or random excitations is worthy of future work for wider benefits during operation; in this regard the development of devices that operate in the off-resonance condition is of interest. In addition, improvements in the configurations of the hydraulic pressure energy harvesting device can act to improve the output performance. This may include the development and selection of new piezoelectric materials that can bear high compressive stresses, or the creation of new configurations by exploring structural and interface benefits. Magnetostrictive materials are particularly suited to operation at high stress and are worthy of future study, and triboelectric approaches have yet to be considered for this application. Moreover, more research is expected to deal with the integration of the HPEH device with power conditioning circuits, energy storage elements, sensors, and control circuits and to conduct the system-level investigations of reliability and stability for the benefits to practical application. Future directions include:

(i) Exploration of new piezoelectric, magnetostrictive or triboelectric materials that can be subjected to higher static and dynamic pressures whilst delivering higher energy harvesting figures of merit, longer life cycles and higher durability. Hard ferroelectric piezoelectric materials will be of interest to explore in more detail, in particular in multi-layer form since it provides opportunities for large length, and low operating voltage and high device capacitance to facilitate power management and impedance matching.

(ii) Novel transducer designs and configurations for power enhancement in low-frequency and broadband energy harvesting in the range of hundreds of hertz for a given volumetric constraint to provide small systems capable of harvesting a range of frequencies.

(iii) The deformation mechanisms of the fluid-to-mechanical interface under a variety of pressure loads need to be further evaluated to optimize the coupling of the transducer material to the pressure ripple and improve device efficiency.

(iv) Current HPEH devices are mostly designed to convert the pressure fluctuations to strain in piezoelectric materials; an alternative direction could be the conversion of pressure

fluctuations to displacements so that electromagnetic transduction could be used, which could increase power.

(v) Current acoustic metamaterials and structures operating in air, and these has the potential to be converted to operate with high pressure hydraulic fluid. This can lead to new designs or geometrical arrangements of the acoustic metamaterials and structures that can operate at the high density fluid mediums of hydraulic systems, which can accommodate the low resonant frequencies.

(vi) Work to date has been limited to relatively low hydraulic pressures, and correspondingly low forces applied to the energy harvesting device, and therefore low harvested energy. It would be of interest to explore high-pressure hydraulic systems, in particular since the power intensity is proportional to the square of the ripple pressure. For example, commercial aircrafts are designed to perform at ~200 bar (about 20 MPa), and therefore high-pressure ripples are expected.

(vii) The lack of standardization of test conditions is an issue, which makes the direct comparison and performance evaluation of different energy harvesting systems difficult.

(viii) Since hydraulic pressure energy harvesting involves converting pressure ripples into electrical energy, some reduction in fluid borne noise or structural borne noise is also expected; this has yet to be investigated in detail and is worthy to study.

(ix) Most work to date has been to laboratory-scale testing and to increase technology readiness level (TRL), there is a need for full system implementation of the hydraulic pressure energy harvesting device with self-powered devices and hydraulic systems.

Acknowledgement

Huifang Xiao would like to thank the support from the National Natural Science Foundation of China under International Cooperation and Exchange Programs with Royal Society [grant number 52111530141]. MP thanks the RAEng/The Leverhulme Trust Senior Research Fellowship, UK [grant number LTSRF1819\15\16] and the RAEng Proof-of-Concept Award PoC1920/15.

References

[1] C. R. Bowen, H. A. Kim, P. M. Weaver, S. Dunn, *Energy Environ. Sci*. **2014**, *7*, 25.

[2] C. F. Wei, X. J. Jing, *Renewable Sustainable Energy Rev.* **2017**, *74*, 1.

[3] Z. B. Yang, S. X. Zhou, J. Zu, D. Inman, *Joule*. **2018**, *2*, 642.

[4] J. Choi, I. Jung, C.Y. Kang, *Nano Energy*. **2019**, *56*, 169.

[5] M. Hamlehdar, A. Kasaeian, M. RezaSafaei, *Renew. Energ*. **2019**, 143, 1826.

[6] F. J. Schwartz, E. A. Skow, A. Erturk, K. A. Cunefare, in *Proc*. *2017 Sensors and Smart Structures Technologies for Civil, Mechanical and Aerospace Systems.* SPIE, Portland **2017**, 1016824.

[7] S. Skaistis, *Noise control for hydraulic machinery*. Taylor & Francis Group, Abingdon, Oxfordshire **1988**.

[8] D. N. Johnston, *Handbook of Noise and Vibration Control, Chapter 76*, Wiley, Hoboken, NJ **2007**.

[9] M. Hughes, *Quieter Fluid Power Handbook. Air Borne Noise from Pipework*, BHRA Fluid Engineering, Cranfield **1981**.

[10] X. R. Zhao, A. Vacca, *Energies*. **2019**, *12*, 535.

[11] D. N. Johnston, *PhD Thesis*, University of Bath **1987**.

[12] K. A. Edge, D. N. Johnston, *Proc. Inst. Mech. Eng., Part A: J. Power Energy*. **1990**, *204*, 33.

[13] K. A. Edge, D. N. Johnston, *Proc. Inst. Mech. Eng., Part A: J. Power Energy*. **1990**, *204*, 41.

[14] ISO 10767-1:1996, *Hydraulic fluid power — Determination of pressure ripple levels generated in systems and components*. **1996**.

[15] ISO 10767-1:2015, *Hydraulic fluid power — Determination of pressure ripple levels generated in systems and components*. **2015**.

[16] C. Yuan, M. Pan, A. Plummer, *J. Dyn. Sys., Meas., Control.* **2020**, *142*, 050801.

[17] M. Pan, C. Yuan, B. Ding, A. Plummer, *J. Dyn. Sys., Meas., Control.* **2021**, *143*(*9*): 091006.

[18] M. Pan, B. Ding, C. Yuan, J. Zou, H. Yang, presented at *Bath/ASME symposium on fluid power and motion control*, Bath, **2018**,

[19] M. Pan, *J. Dyn. Sys., Meas., Control.* **2017**, *139*, 081007.

[20] M. Pan, N. Johnston, A. Plummer, *J. Phys.: Conf. Ser*. **2016**, *744*, 012016.

[21] M. Pan, A. Hillis, N. Johnston, presented at *10th UKACC International Conference on Control*, Loughborough, October **2014**.

[22] M. Pan, N. Johnston, A. Hillis, *Proc. Inst. Mech. Eng., Part I: J. Systems and Control Engineering*. **2013**, *227*, 610.

[23] P. Gao, T. Yu, Y. Zhang, J. Wang, J. Zhai, *Chin. J. Aeronaut*. **2021**, *34*, 83.

[24] V. Bhatnagar, P. Owende, *Energy Sci. Eng*. **2015**, 153.

[25] A. Erturk, K.A. Cunefare. US. US010211761B2, **2019**.

[26] K. A. Cunefare, E. A. Skow, A. Erturk, J. Savor, N. Verma, M. R. Cacan, *Smart Mater. Struct*. **2013**, *22*, 025036.

[27] N. Verma, E. A. Skow, K. A. Cunefare, A. Erturk, in *Proc. 2013 Conference on Smart Materials, Adaptive Structures and Intelligent Systems*, ASME, Snowbird **2013**.

[28] E. A. Skow, K. A. Cunefare, A. Erturk, *Smart Mater. Struct*. **2014**. *23*, 104011.

[29] E. A. Skow, K. A. Cunefare, A. Erturk, in *Proc. 2014 International Mechanical Engineering Congress and Exposition*, ASME, Canada **2014**, 4.

[30] M. F. Toothman, E. Ting, E. A. Skow, K. A. Cunefare, in *Proc. 2018 Sensors and Smart Structures Technologies for Civil, Mechanical, and Aerospace Systems* SPIE, Denver **2018**, 105980R.

[31] Y. Liu, Z. Xu, L. Hua, X. Zhao, *Energy Convers. Manage*. **2020**, *221*, 113196.

[32] Q. Nie, H. Nie, M. Zhang, *Machine tool and hydraulics*. **2012**, *40*, 80.

[33] K. A. Cunefare, E. A. Skow, A. Erturk, in *Proc. Meetings on Acoustics*, Canada **2013**, 19.

[34] J. J. Allen, A. J. Smits, *J. Fluid Struct*. **2001**, *15*, 629.

[35] D. St. Clair, A. Bibo, V. R. Sennakesavababu, M. F. Daqaq, G. Li, *Appl. Phys. Lett.* **2010**, *96*, 144103.

[36] T. B. Xu, E. Siochi, J. Kang, L. Zuo, W. Zhou, X. Tang, X. Jiang, in *Proc. ASME Design Engineering Technical Conference*, Washington **2011**, 1.

[37] T. B. Xu, E. J. Siochi, J. H. Kang, L. Zuo, W. Zhou, X. Tang, X. Jiang, *Smart Mater. Struct.* **2013**, *22*.

[38] F. Qian, T. B. Xu, L. Zuo, *Eng. Struct.* **2018**, *173*, 191.

[39] J. J. L. Aranda, B. Oelmann, S. Bader, presented at *IEEE International Conference on Advanced Intelligent Mechatronics* (*AIM*), Munich **2017**.

[40] S. H. Lu, F. Boussaid, *IEEE Trans. Power Electron*. **2015**, *30*, 10.

[41] D. Alghisi, V. Ferrari, M. Ferrari, D. Crescini, F. Touati, A. B. Mnaouer, *Sens. Actuators, A*. **2017**, *234*, 246.

[42] F. Qian, Y. B. Liao, L. Zuo, P. Jones, *Mech. Syst. Signal Process*. **2021**, *151*, 10740.

[43] Z. W. Zhang, H. J. Xiang, L. H. Tang, *Mech. Syst. Signal Process*. **2021**, *152*, 107476.

[44] D. X. Cao, X. J. Duan, X. Y. Guo, S. K. Lai, *Sens. Actuators, A*. **2020**, *309*, 112031.

[45] E. A. Skow, *PhD Thesis*, Georgia Institute of Technology **2017**.

[46] J. Cullman, H. Zhang, J. Howland, Z.S. Jiang, N. White, Eur. EP3619790B1, **2021**.

[47] J. L. Aranda, S. Bader, B. Oelmann, presented at *44th Annual Conference of the IEEE Industrial Electronics Society*, Washington **2018**.

[48] J. J. L. Aranda, S. Bader, B. Oelmann, *Sens. Actuators, A*. **2019**, *291*, 58.

[49] J. Fraden, *Handbook of Modern Sensors: Physics, Designs, and Applications*, Springer-Verlag, New York **2015**.

[50] J. J. L. Aranda, S. Bader, B. Oelmann, *IEEE Trans. Instrum. Meas*. **2018**, *67*, 2705.

[51] S. Way, *Transactions of the American Society of Mechanical Engineers Applied Mechanics*, **1934**, *56*, 627.

[52] M. Sheplak, J. Dugundji, *J. Appl. Mech*. **1998**, *65*, 107.

[53] H. Xue, H. P. Hu, *IEEE Trans. Ultrason. Eng*. **2008**, 55, 2092.

[54] D. Karagiozova, T. X. Yu, S. Y. Shi, L. Zhu, *Int. J. Mech. Sci*. **2017**, *131*, 894.

[55] H. F. Xiao, H. T. Qie, B. Chris, *Mech. Syst. Signal Process*. 2021, *146*, 107013.

[56] S. Pryia, *IEEE Trans. Ultrason. Eng*. **2010**, *57*.

[57] K. Uchino, *Energy Technol*. **2018**, 6829.

[58] J. I. Roscow, H. Pearce, H. Khanbareh, S. Kar-Narayan, C. R. Bowen, *Eur. Phys. J.: Spec. Top*. **2019**, *228*, 1537.

[59] D. A. V. D. Ende, H. J. V. D. Wiel, W. A. Groen, S. V. D. Zwaag, *Smart Mater. Struct*. **2012**, *21*, 015011.

[60] D. Damjanovic, *Curr. Opin. Solid State Mater. Sci*. **1998**, *3*, 469.

[61] D. Belincout, H. H. A. Kruger, *Properties of Morgan Electro ceramic ceramics*,

Technical Publication TP-226.

[62] http://www.trstechnologies.com/Materials/High-Performance-PMN-PT-Piezoelectric-Single-Crystal

[63] S. J. Zhang, F. Li, *J. Appl. Phys.* **2012**, *111*, 031301.

[64] H. C. Cao, A. G. Evans, *J. Am. Ceram. Soc*. **1993**, *76*, 890.

[65] M. W. Hooker. Properties of PZT-based piezoelectric ceramics between -150 and 250 ºC, NASA/CR-1998-208708, **1998**.

[66] D. A. HALL, *J. Mater. Sci*. **2001**, *36*, 4575.

[67] W. D. Dong, P. Finkel, A. Amin, C. S. Lynch, *Appl. Phys. Lett*. **2012**, *100*, 042903.

[68] G. Vats, S. Patel, A. Chauhan, R. Vaish, *Int. J. Appl. Ceram. Technol*. **2015**, *12*, 765.

[69] R. B. Olsen, D. Evans, *J. Appl. Phys*. **1983**, *54*, 5941.

[70] Z. X. Deng, M. J. Dapino, *Smart Mater. Struct*. **2017**, *26*, 055027.

[71] F. Narita, M. Fox, *Adv. Eng. Mater*. **2018**, *20*, 1700743.

[72] L. Wang, F. G. Yuan, *Smart Mater. Struct*. **2008**, *17*, 045009.

[73] S. Greco, A. Lange, B. Kirsch, *Procedia CIRP*, **2019**, *82*, 160.

[74] T. H. Cheng, Q. Gao, Z. L. Wang, *Adv. Mater. Technol*. **2019**, 1800588.

[75] S. Chandrasekaran, C. Bowen, J. Roscow, Y. Zhang, D. K. Dang, E. J. Kim, R.D.K. Misra, L. Deng, J. S. Chung, S. H. Hur, *Phys. Rep*. **2019**, *792*, 1.

[76] M. P. Kim, D. S. Um, Y. E. Shin, H. Ko, *Nanoscale Res. Lett.* **2021**, 16.

[77] L. Dong, C. R. Jin, A. B. Closson, I. Trase, H. C. Richards, Z. Chen, J. X. J. Zhang, *Nano Energy*. **2020**, *76*, 105076.

[78] Z. L. Wang, W. Wu, *Angew. Chem. Int. Ed*. **2012**, *51*, 11700.

[79] C. S. Wu, R. Y. Liu, J. Wang, Y. L. Zi, L. Lin, Z. L. Wang, *Nano Energy*. **2017**, *32*, 287.

[80] D. H. Zhang, J. W. Shi, Y. L. Si, T. Li, *Nano Energy*. **2019**, *61*, 132.

[81] A. Ahmed, I. Hassan, A. S. Helal, V. Sencadas, A. Radhi, C. K. Jeong, M. F. El-Kady, *iScience*. **2020**, *23*, 101286.

[82] J. X. Zhong, S. Qian, X. G. Wang, C. J. Yang, J. He, X. J. Hou, X. J. Chou, *Mater. Lett.* **2020**, *306*, 130859.

[83] J. Yang, J. Chen, Y. Liu, W. Yang, Y. Su, Z. L. Wang, *ACS Nano*. **2014**, 2649.

[84] N. Cui, L. Gu, J. Liu, S. Bai, J. Qiu, J. Fu, X. Kou, H. Liu, Y. Qin, Z. L. Wang, *Nano*

Energy. **2015**, *15*, 321.

[85] F. Chen, Y. Wu, Z. Ding, X. Xia, S. Li, H. Zheng, C. Diao, G. Yue, Y. Zi, *Nano Energy*. **2019**, *56*, 241.

[86] H. F. Zhao, X. Xiao, P. Xu, T. C. Zhao, L. G. Song, X. X. Pan, J. C. Mi, M.Y. Xu, Z. L. Wang, *Adv. Energy Mater*. **2019**, *9*, 1902824.

[87] M. Yuan, C. H. Li, H. M. Liu, Q. H. Xu, Y. N. Xie, *Nano Energy*. **2021**, *85*, 105962.

[88] L. Kela, *Arch. Appl. Mech*. **2009**, *79*, 1115.

[89] N. E. Earnhart, K. A. Cunefare, *Int. J. Fluid Power*. **2012**, *13*, 41.

[90] Y. Xi, B. R. Li, L. L. Gao, T. F. Tang, H. L. Liao, *Applied Acoustics*. **2018**, *134*, 131.

[91] M. Yuan, Z. P. Cao, J. Luo, X. J. Chou, *Micromachines*. **2019**, *10*, 48.

[92] Q. B. Mao, S. Q. Li, W. W. Liu, *Appl. Acoust*. **2018**, *141*, 348.

[93] J. S. Chen, Y. B. Chen, Y. H. Cheng, L. C. Chou, *Phys. Lett. A*. **2020**, *384*, 126887.

[94] E. A. Skow, Z. Koontz, K.A. Cunefare, A. Erturk, in *Proc. 2015 Active and Passive Smart Structures and Integrated Systems* (Eds: W. H. Liao, G. Park, A. Erturk), SPIE, California **2015**, 9431.

[95] N. E. Earnhart, *PhD Thesis*, Georgia Institute of Technology **2012**.

[96] F. Qian, T. B. Xu, L. Zuo, *Energy Convers. Manage*. **2018**, *171*, 1352.

[97] X. Wang, Z. Shi, J. Wang, H. Xiang, *Smart Mater. Struct*. **2016**, *25*, 055005.

[98] W. Chen, Y. Wang, W. Deng, *J. Intell. Mater. Syst. Struct*. **2017**, *28*, 827.

[99] M. Evans, L. Tang, K. C. Aw, *J. Intell. Mater. Syst. Struct*. **2018**, *29*, 1941.

[100] J. Cho, R. Richards, D. Bahr, C. Richards, M. Anderson, *Appl. Phys. Lett*. **2006**, *89*, 104107.

[101] L. Wang, S. Chen, W. Zhou, T. B. Xu, L. Zuo, *J. Intell. Mater. Syst. Struct.* **2017**, *28*, 1175.

[102] Y. Kuang, Z. J. Chew, J. Dunville, J. Sibson, M. Zhu, *Energy Convers. Manage*. **2021**, *237*, 114129.

[103] Y. Kuang, Z. J. Chew, M. Zhu, *Energy Convers. Manage*. **2020**, *213*, 112855

[104] M. H. Khairuddin, M. F. M. Said, A. A. Dahlan, K. A. Kadir, *Arch. Acoust*. **2018**, *43*, 369.

[105] Z.S. Chen, B. Guo, Y. M. Yang, C.C. Cheng, *Phys. B*. **2014**, *438*, 1.

[106] Z. Yang, H. M. Dai, N. H. Chan, G. C. Ma, P. Sheng, *Appl. Phys. Lett.* **2010**, *96*, 041906.

[107] Z. Liu, X. Zhang, Y. Mao, Y.Y. Zhu, Z. Yang, C.T. Chan, P. Sheng, *Phys. B*. **2020**, *338*, 201.

[108] M. Yuan, Z. P. Cao, J. Luo, R. Ohayon, *J. Low Freq. Noise Vib. Act. Control*. **2018**, *37*, 1015.

[109] K. H. Sun, J. E. Kim, J. Kim, K. J. Song, *Smart Mater. Struct*. **2017**, *26*, 075011.

[110] X. L. Wang, J. J. Xu, J. J. Ding, C. Y. Zhao, Z. Y. Huang, *Smart Mater. Struct*. **2019**, *28*, 025035.

[111] J. F. Li, X. M. Zhou, G. L. Huang, G. K. Hu, *Smart Mater. Struct*. **2016**, *25*, 045013.

[112] N. Gao, J. Wu, H. Hou, L. Yu, *Int. J. Mod. Phys. B*. **2017**, *31*,1750011.

[113] E. A. Skow, K. A. Cunefare, A. Erturk, in *Proc. 2013 Active and Passive Smart Structures and Integrated Systems* (Eds: H. A. Sodano), SPIE, California **2013**, 8688.

[114] J. L. Aranda, S. Bader, B. Oelmann, *Sens. Actuators, A*. **2021**, *21*, 1546.

[115] H. Liu, R. Hua, Y. Lu, Y. Wang, E. Salman, J. Liang, *J. Intell. Mater. Syst. Struct*. **2019**, *30*, 813.